

# Development of a Variable Deceleration Rate Approach to Rollover Crash Reconstruction

Nathan A. Rose, Gray Beauchamp  
Kineticorp, LLC

Copyright © 2009 SAE International

## ABSTRACT

The goal of this paper is to advance rollover crash reconstruction techniques beyond the assumption typically made that a rolling vehicle decelerates at a constant rate. The paper presents and applies a planar vehicle-to-ground impact model to explore the manner in which a vehicle's deceleration rate would be expected to vary over the course of a rollover. Based on this analysis, several possible variable deceleration rate profile shapes are then suggested for rollover crash reconstruction. Then, two rollover crash tests are analyzed to determine the extent to which these suggested variable deceleration rate profiles can be expected to yield accurate reconstructions of the translational and angular velocity histories for actual rollovers. Overall, each of the suggested variable deceleration rate profiles represented a significant improvement over using a constant deceleration rate.

## INTRODUCTION

Calculations carried out to determine a rolling vehicle's<sup>1</sup> over-the-ground (OTG) speed have typically assumed that the vehicle decelerated at a constant rate. The technical literature related to rollover reconstruction has reported average deceleration rates for rolling vehicles that vary between 0.36 and 0.65g [3, 5, 16, 17, 18, 19, 21, 22, 25, 31]. Until recently, though, none of the literature reporting these deceleration rates has discussed how they vary over the course of the rollover.

<sup>1</sup> Throughout this paper, the phrase "rolling vehicle" should be taken to refer to a vehicle in the midst of a rollover, not a vehicle that is rolling on its wheels.

It is intuitive that the deceleration rate of a rolling vehicle varies over the distance of the roll. Empirical data has supported this intuition. Recently, several researchers have reported specific crash tests and real-world rollovers in which the deceleration rate was higher during the early portions of the rollover than during the later portions [1, 9, 15]. For instance, Reference 1 reported analysis of a real-world rollover that was captured on video. This analysis showed that the vehicle's deceleration rate during the rollover was non-constant, that it was highest early in the roll, and that it varied between 0.6 and 0.2 g over the course of the roll. Though not explicitly discussing the variability of the deceleration rate over the roll distance, other authors have noted that wheel-to-ground impacts have the potential of producing higher deceleration rates than roof-to-ground impacts. Orłowski observed that "tire/wheel impacts are capable of causing higher and more sustained deceleration of the vehicle than the roof structure would for a comparable impact...As a result, tire/wheel impacts cause a higher change in velocity..." [24].

In Reference 9, Carter examined the accuracy of using a constant deceleration rate for rollover reconstruction by comparing crash test data to reconstructed results. For the two rollover crash tests that he examined, Carter found that the vehicles' deceleration rates were not constant over the roll distance and that they were higher during the early portions of the rolls than during the later. Thus, when using a constant deceleration approach, the deceleration rates for the early portions of the rolls were underestimated and those during the later portions were overestimated. For the two cases examined by Carter, the constant deceleration approach overestimated the

The Engineering Meetings Board has approved this paper for publication. It has successfully completed SAE's peer review process under the supervision of the session organizer. This process requires a minimum of three (3) reviews by industry experts.

All rights reserved. No part of this publication may be reproduced, stored in a retrieval system, or transmitted, in any form or by any means, electronic, mechanical, photocopying, recording, or otherwise, without the prior written permission of SAE.

ISSN 0148-7191

Positions and opinions advanced in this paper are those of the author(s) and not necessarily those of SAE. The author is solely responsible for the content of the paper.

**SAE Customer Service:** Tel: 877-606-7323 (inside USA and Canada)  
Tel: 724-776-4970 (outside USA)  
Fax: 724-776-0790  
Email: [CustomerService@sae.org](mailto:CustomerService@sae.org)

**SAE Web Address:** <http://www.sae.org>

Printed in USA

**SAE**International™

vehicles' OTG speeds at most discrete points along the roll distances.

In rollover reconstruction, estimates of a vehicle's roll velocity history are obtained by determining roll positions at discrete points along the roll path and then estimating the time that elapsed while the vehicle traversed the distance between these positions. Since the deceleration rate influences these time estimates, it will also influence the roll velocities that are obtained. Thus, using the constant deceleration approach can also introduce errors into estimates of the roll velocity history. Carter [9] found that the accuracy of the constant deceleration approach depended on the number of roll positions that could be established during the roll phase, but in general, the constant deceleration approach tended to overestimate the peak roll velocities.

It is clear from Carter's research that the accuracy of reconstructed translational and roll velocity histories for rollovers could be improved if reconstructionists were able to prescribe physically realistic variations in a rolling vehicle's deceleration rate. By developing an understanding of how a rolling vehicle's instantaneous deceleration rate varies over the course of the roll distance, analysts could achieve greater accuracy in calculating instantaneous translational and angular velocities at discrete points along the roll path. The accuracy of these instantaneous velocities becomes relevant and significant when one begins to consider a rollover on an event-by-event basis, considering each ground impact and airborne phase as a discrete event [26, 27, 28], and when one uses mathematical models to analyze occupant dynamics [2, 12, 13, 14, 23].

To date, there has been virtually no published research that has explored how a rolling vehicle's instantaneous deceleration rate will vary over the roll distance. Some authors have made empirical observations related to these topics based on particular crash tests or real-world rollovers [1, 9, 15, 19]. It should be observed, though, that a coherent and logically justified approach to treating a rollover as a multi-phase event cannot be developed without some theoretical underpinning that would allow one to generalize from the results of specific crash tests to conclusions about what is true of rollovers, in general, and what would likely be true in a particular rollover that does not exactly resemble the available crash test data.

The authors can envision several potentially viable analytical approaches for estimating the variability of the deceleration rate of a rolling vehicle over the course of the roll distance. The first of these, we will term the "discrete event approach". In this approach, one would first determine the discrete distances over which the rolling vehicle was in contact with the ground and those distances over which it was airborne. Then, the analyst would either use empirical data or an impact model, such as the one treated in this paper, to determine a

deceleration rate for each ground contact. Simulation could also be a potentially useful tool for this purpose. The deceleration rate for each airborne phase would be set to zero. This would result in a deceleration rate history that would, conceptually, look something like that in Figure 1.<sup>2</sup>

In the graph of Figure 1, we have plotted distance on the horizontal axis and the deceleration rate on the vertical axis. This graph depicts a rollover with four discrete ground contact phases having deceleration rates  $f_1$ ,  $f_2$ ,  $f_3$  and  $f_4$ .

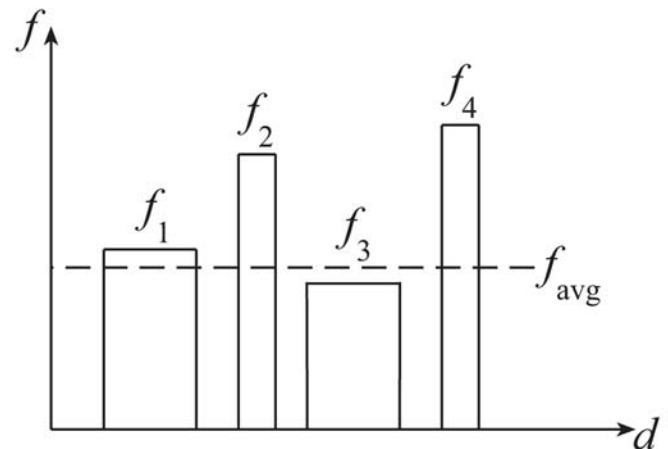


Figure 1

This discrete event approach appears to be what Carter had in mind in his comments in the discussion of Reference 9: "...it was apparent that there are phases of the roll event where the vehicle is in contact with the ground and decelerating and there are phases where the vehicle is in the air and maintaining a more-or-less constant OTG speed. In the field, given enough evidence, it may be possible to define, within reason, both phases throughout the roll sequence. Then, using a multiphasic approach, it may be possible to develop a more realistic distance history of OTG speed. Further, it may be possible to more accurately define the time intervals during the roll sequence, and thereby generate roll rate histories that more closely match the actual event."

It is true that, given sufficient evidence, a skilled reconstructionist could define distances over which a vehicle is in contact with the ground and distances over which it is airborne. However, in general, a discrete events approach would still present substantial challenges. First, there will be many cases when the documented evidence is insufficient to delineate each ground contact and airborne phase. Not only that, once the ground contact regions were identified, the analyst would need some means of linking the impact conditions to the deceleration rate for that impact. This process would likely be rather time consuming and would involve

<sup>2</sup> Figure 1 depicts constant deceleration rates for each impact. Using simulation, one could potentially prescribe a variable deceleration rate for each discrete impact.

analytical impact modeling or simulation. Further, this process would be iterative since the deceleration rate for a ground impact would depend on the vehicle's OTG speed, the very quantity that the analyst is attempting to calculate. These difficulties could be resolved with further research and this approach is likely to receive attention in the upcoming literature of rollover accident reconstruction.

A second approach, which given the current state of rollover reconstruction techniques seems more viable than the first, will be termed the "discrete regions approach". In this approach, one would not need to precisely parse out each discrete event that occurs during the rollover (though one might have other reasons for doing so). Instead, the analyst would vary the deceleration rate in a sequence of regions, as depicted in Figure 2. This graph depicts a rollover consisting of three regions, each having a different average deceleration rate. One or more of the regions could also be assigned a non-constant deceleration rate – say for instance, Region 2 could be assigned a linearly decreasing deceleration rate that links a high deceleration rate in Region 1 to a low deceleration rate in Region 3. Or, perhaps, Region 1 could be assigned a constant deceleration rate and a linearly decreasing deceleration rate could then traverse both Regions 2 and 3.

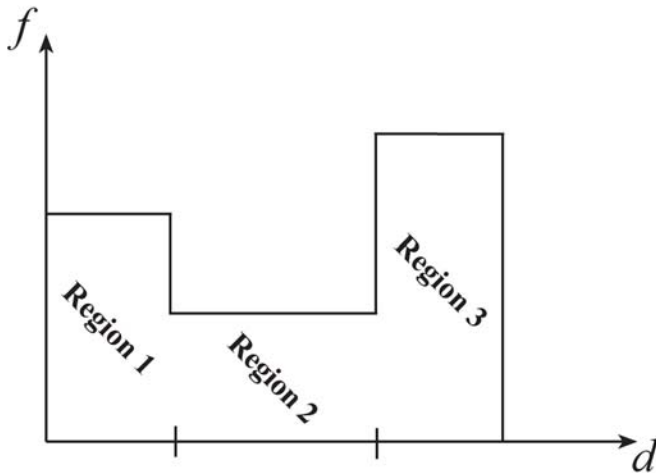


Figure 2

To use this approach, one would need to decide what criteria to use to identify and separate the regions. Much of this paper will focus on a rationale for identifying regions between which a rolling vehicle's deceleration rate would vary. We will show that a vehicle's roll velocity history reveals such regions in which the vehicle's deceleration rate would vary and provides the necessary information for delineating these regions in a manner that has physical meaning.

A third approach, which we'll term the "continuously variable approach", would involve specifying the variability of the deceleration rate over the course of a rollover with a continuous function. The simplest assumption for this approach would be to assume the

deceleration rate decreases linearly with the roll distance as shown in Figure 3. With this assumption, the analyst would either specify the initial and final deceleration rates or the initial deceleration rate and the rate at which it decreases. This approach would be simple to implement and it will be explored in this paper along side the discrete regions approach. This approach is essentially a modified version of the second approach, in which the region-by-region variation in the vehicle's deceleration rate is accomplished with a continuous function.

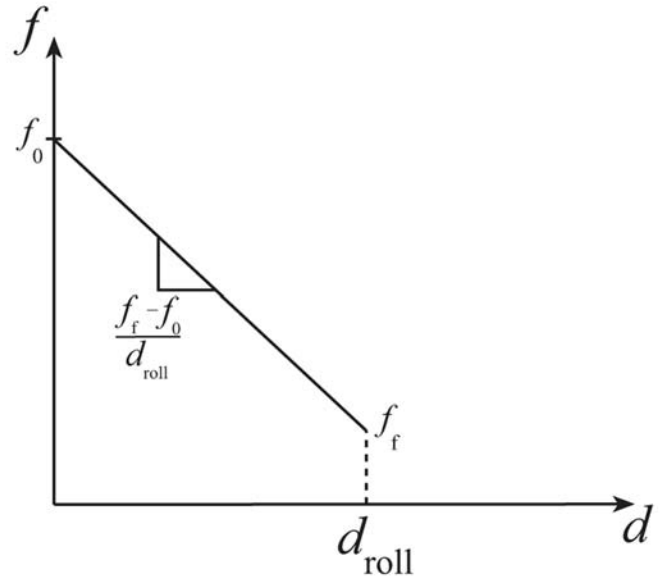


Figure 3

## PREVIEW OF CONCLUSIONS

Though empirical data will be discussed extensively in this paper, a large portion of the discussion is slanted towards developing a coherent theory that would provide the basis for a variable deceleration rate approach to rollover accident reconstruction. In developing this theory, we draw heavily on planar impact mechanics, which is introduced most systematically in Reference 4. For readers unacquainted with planar impact mechanics, Reference 4 will provide useful background discussion, particularly related to the critical impulse ratio concept that is used extensively in this paper.

At any rate, in the spirit of getting to the point, we offer the following preview of the conclusions at which this paper ultimately arrives.

1. A typical high-speed rollover can be divided into the following three regions related to the vehicle's roll velocity history: (1) a region during which the vehicle's roll velocity builds up to its peak region; (2) a region in which the vehicle's roll velocity plateaus, with the vehicle experiencing either small increases or decreases in roll velocity; (3) and a region in which the vehicle's roll velocity decreases more significantly until the roll motion of the vehicle terminates. Some rollovers lack a clearly defined region in which the roll velocity plateaus (Region

2) [9, 10], but these can be seen as special cases of the more general three-region behavior of the typical roll velocity history.

2. These three regions of the roll velocity history reflect changes in the physics of a rollover that occur as the vehicle's OTG speed decreases. Region 1 is generally associated with high OTG speeds, Region 2 with moderate OTG speeds, and Region 3 with low OTG speeds.

3. The underlying physics that causes this three-region behavior in the roll velocity history will also manifest itself in the rate at which the vehicle decelerates over the course of the rollover. Assuming a constant available surface friction coefficient, a rolling vehicle's deceleration rate will generally be highest in Region 1 and lowest in Region 3. In other words, a rolling vehicle's deceleration rate will generally decrease as it progresses through the three regions.

4. Variations in the available surface friction can cause variations in this general trend of a deceleration rate that decreases as the vehicle progresses through the roll. Variations in the available surface friction can be caused by changes in the properties of the surface on which the vehicle is rolling (i.e., moving from asphalt to dirt) or by changes in the way the vehicle engages the surface on which it is rolling (i.e., a rim digging into the surface will have higher "friction" associated with it than a roof rolling smoothly over the same surface).

5. The coefficient of friction between the rolling vehicle and the surface on which it is rolling will influence the deceleration rate of the vehicle. The structural properties of that surface and the manner in which the vehicle engages that surface will influence that coefficient of friction [19].

6. Implementing a variable deceleration rate approach to rollover reconstruction would involve the following steps:

- a. Spatially reconstruct the motion of the vehicle based on physical evidence deposited at the crash scene and on the crash vehicle.
- b. Use a constant deceleration rate to generate an initial estimate of the OTG speed versus distance and roll velocity versus distance curves.
- c. Identify the three (or two) regions of the roll velocity distance history in terms of the roll distance.
- d. Generate a variable deceleration rate profile that will yield the same average deceleration rate with which the initial estimate curves were generated. Multiple shapes, which are discussed in this paper, are available for this profile (e.g., a step function with a different constant deceleration rate for each zone or

a continuous function that yields a smooth variation in the deceleration rate).

The variable deceleration rate profile generated in this step should be setup consistent with the basic principles laid out in this paper, but also consistent with the specific details of the particular case being reconstructed. For instance, this paper will show that for a surface of constant friction the vehicle's OTG deceleration rate will tend to decrease as the rollover progresses. However, if the vehicle rolls across multiple surfaces, this trend may not be realized. The real-world rollover analyzed in Reference 1 had a higher deceleration rate in the later stage of the rollover once it had rolled onto a grass and dirt surface than it did in the middle stage of the rollover when it was still rolling on asphalt.

- e. Having generated a variable deceleration rate profile, recalculate the speed versus distance and roll velocity versus distance curves using the variable deceleration rate profile.

## **ANALYZING VEHICLE-TO-GROUND IMPACTS**

A rollover crash consists of a series of vehicle-to-ground impacts separated by periods of airborne motion. The specific conditions of the impacts - including the initial velocities, the orientation and geometry of the impact, and the vehicle's inertial and structural properties - will determine the forces to which the vehicle is subjected. These forces will, in turn, determine the specific motion that the vehicle exhibits. Thus, the rate at which a rolling vehicle decelerates along the ground will be determined by the accumulation of the ground plane forces that are applied to the vehicle during the rollover. Any factor that influences the ground plane forces would also be expected to influence the deceleration rate that the vehicle experiences during a particular vehicle-to-ground impact and, potentially, over the course of the entire rollover.

Several previous papers [26, 27, 28] have reported analysis with a planar, impulse-momentum, vehicle-to-ground impact model based on the idealized vehicle-to-ground impact shown in Figure 4. This model can provide a theoretical context in which to explore those factors that will influence the ground plane forces applied to a vehicle during a rollover, and thus, those factors that will influence its deceleration rate.

The vehicle in Figure 4 is depicted in an inverted orientation with the driver's side roof impacting the ground. The vehicle has velocity both along and into the ground and a roll velocity that contributes to the speed with which the roof impacts the ground. As a result of this impact, the vehicle is subjected to an impact force that consists of both vertical and ground surface components. The geometry of the impact is defined by the impact radius, which is the distance from the vehicle

center-of-mass (CoM) to the point at which the impact force is applied, and the impact angle, which is the angle between the ground plane and the impact radius. Though depicted as a roof-to-ground impact in Figure 4, the equations of this impact model are equally applicable to other types of vehicle-to-ground impacts, such as wheel-to-ground impacts.

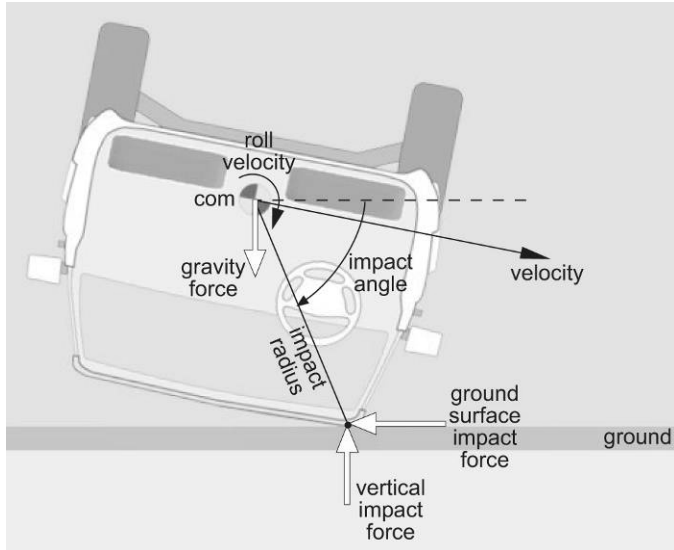


**Figure 4**

Figure 5 again depicts this idealized impact between a vehicle and the ground. In this figure, the descriptive labels of the previous figures have been replaced with the symbols which are used in the impact model equations. The impact angle and impact radius are designated with the symbols  $\phi$  and  $r$ . The velocity vector is designated with the letter  $v$  and the vehicle's roll velocity is designated  $\omega_r$ . During the depicted impact, the vehicle is subjected to both upward and ground surface impact force components,  $F_{\text{vertical}}$  and  $F_{\text{ground}}$ , and the gravity force, which is the vehicle's weight. In general,  $F_{\text{ground}}$  can act in either the positive (left) or negative (right) direction.

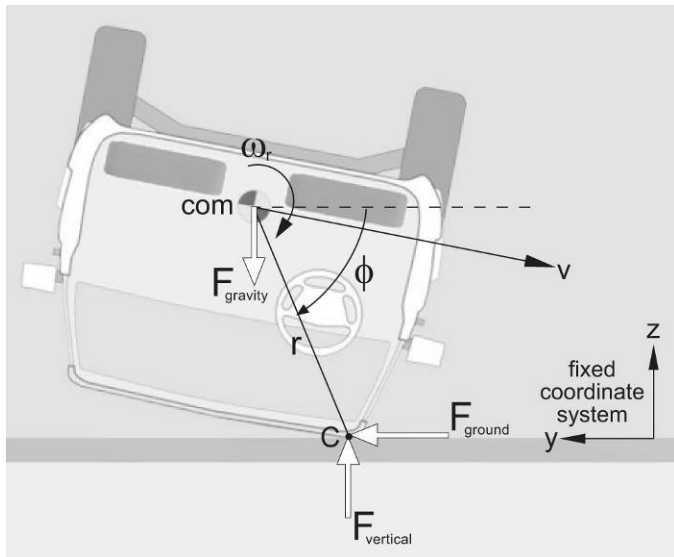


**Figure 5**

In developing the equations for this impact model, the following assumptions were invoked:

1. The impact was assumed to occur entirely in a single plane, and thus, velocity changes along the vehicle's longitudinal axis are neglected, as are changes in pitch and yaw velocity.
2. The impact model equations recognize no change in the position of the vehicle through the impact. This is not to say that the model cannot be used to analyze a vehicle-to-ground impact during which significant vehicle rotation occurs. When analyzing such an impact with this model, though, the analyst would need to select a vehicle position and orientation that would be most representative of the vehicle's position and orientation through the impact. Reference 27 discusses this issue.
3. The impact force was assumed to be concentrated at a single point. This point is assumed to lie a fixed distance ( $r$ ) from the vehicle's center-of-mass. Mathematically, this is a rigid body assumption. Nonetheless, to some degree, effects of vehicle deformation can be included in analysis with this model. To incorporate deformation effects, the analyst would define an impact radius and impact angle that reflect the deformed shape of the vehicle. The effect of deformation on the impact angle and radius was discussed briefly in Reference 28.
4. It was assumed that no moment arises at the contact point.
5. Any effects of ground plane restitution have been neglected. In other words, the ground surface impact force was assumed to be a frictional, or retarding, force that depends on relative velocity at the contact point for its development. It is assumed that there is no structural restitution that could potentially cause a velocity reversal in the contact region [4, 27]. Restitution normal to the ground plane is included in the model.

Application of the principle of impulse and momentum for the idealized impact of Figure 5 results in the following equations, which yield the vehicle's upward and ground plane CoM velocity changes ( $\Delta V_z$  and  $\Delta V_y$ ) and the vehicle's change in roll velocity ( $\Delta \omega_r$ ). The derivation of these equations is provided in Appendix A of Reference 28.

$$\Delta V_z = (1 + e) \cdot v_{z,i} \cdot \left\{ \frac{k_r^2}{r^2 \cdot c \phi \cdot (\mu \cdot s \phi - c \phi) - k_r^2} \right\} \quad (1)$$

$$- g \cdot \Delta t \cdot \left\{ \frac{r^2 \cdot c \phi \cdot (\mu \cdot s \phi - c \phi)}{r^2 \cdot c \phi \cdot (\mu \cdot s \phi - c \phi) - k_r^2} \right\}$$

$$\Delta V_y = \mu \cdot (\Delta V_z + g \cdot \Delta t) \quad (2)$$

$$\Delta\omega_r = (\Delta V_z + g \cdot \Delta t) \cdot \frac{r \cdot (\mu \cdot s\phi - c\phi)}{k_r^2} \quad (3)$$

In these equations,  $v_{z,c,i}$  is the vertical velocity of the vehicle at Point C immediately preceding the ground contact,  $k_r$  is the vehicle's radius of gyration for the roll axis,  $g$  is the gravitational constant,  $\Delta t$  is the duration of the impact, and the letters  $s$  and  $c$  designate the sine and cosine. Although the collision force has been assumed to be transferred without any movement of the vehicle, accounting for the effect of the gravity impulse has required inclusion of the impact duration.

The initial vertical velocity at Point C,  $v_{z,c,i}$ , is given by the following equation:

$$v_{z,c,i} = v_{z,i} - r \cdot c\phi \cdot \omega_{r,i} \quad (4)$$

Equations (1) through (3) also include the coefficient of restitution,  $e$ , and the impulse ratio,  $\mu$ . The coefficient of restitution is the negative ratio of the post-impact to the pre-impact vertical velocity at Point C. The impulse ratio is the ratio of the ground plane collision impulse to the vertical direction collision impulse. In many instances, the impulse ratio can be thought of as a coulomb friction value [29], though its application is not limited to this interpretation [5, 6, 7, 8, 20, 28].

In addition to the effects of friction between the ground and the vehicle body, the ground plane impulse will also include the effects of forces generated by snagging between the vehicle and the ground or furrowing of the vehicle into the ground. The "available friction" would be set at a value that reflects such snagging or furrowing when it occurs. For example, a coefficient of friction of 0.5 may reasonably represent the available friction when a vehicle body is sliding on asphalt. But, if a wheel rim gouges into the asphalt, the "available friction" coefficient may need to be set significantly higher than 0.5 to represent the ground plane force arising from the mechanical engagement between the rim and the asphalt [29, 30]. The same would likely be true for some portion of the vehicle gouging or furrowing into soil. The "available friction" for such engagement would likely be much higher than for the vehicle body simply sliding on the surface of the soil [11].

Within the impact model, the sign of the impulse ratio governs the direction in which the ground plane collision force acts. A positive impulse ratio produces a ground plane force that acts in the positive direction and a negative impulse ratio results in a ground plane force that acts in the negative direction. The direction of the ground plane impact force, in turn, determines whether the vehicle will experience a positive or negative ground plane velocity change and whether the ground surface impact force will tend to increase or decrease the roll velocity.

Physically, the ground plane impulse will act in a direction opposing the velocity of the vehicle in its region of contact with the ground (Figures 6a and 6b). Thus, the impulse ratio can be further specified with the following equation:

$$\mu = -\mu_0 \cdot \text{sign}(v_{y,c,i}) \quad (5)$$

In this equations,  $\mu_0$  is the nominal value of the impulse ratio that defines the magnitude of the ground plane impulse relative to the vertical impulse and  $v_{y,c,i}$  is the ground plane velocity of the vehicle at Point C.

This velocity is given by the following equation:

$$v_{y,c,i} = v_{y,i} + r \cdot s\phi \cdot \omega_{r,i} \quad (6)$$

Thus, for a particular vehicle-to-ground impact, the signs and relative magnitude of the vehicle's CoM ground plane velocity ( $v_{y,i}$ ) and the ground plane component of its rotational perimeter velocity ( $r \cdot s\phi \cdot \omega_{r,i}$ ) will determine the sign of  $v_{y,c,i}$  and, thus, the sign of  $\mu$ .

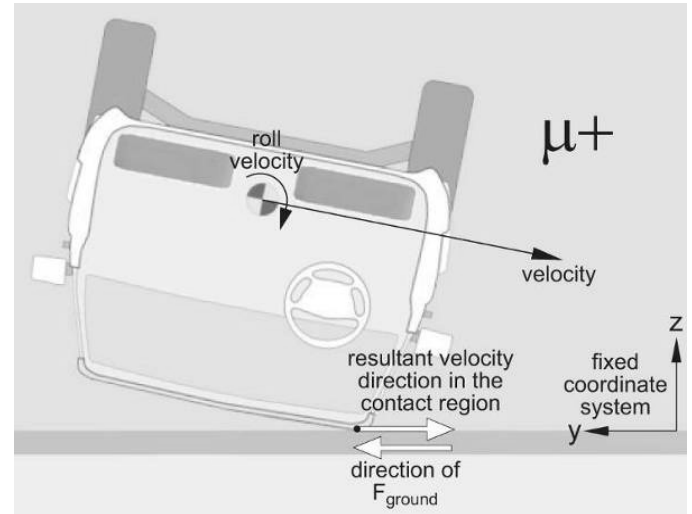


Figure 6a

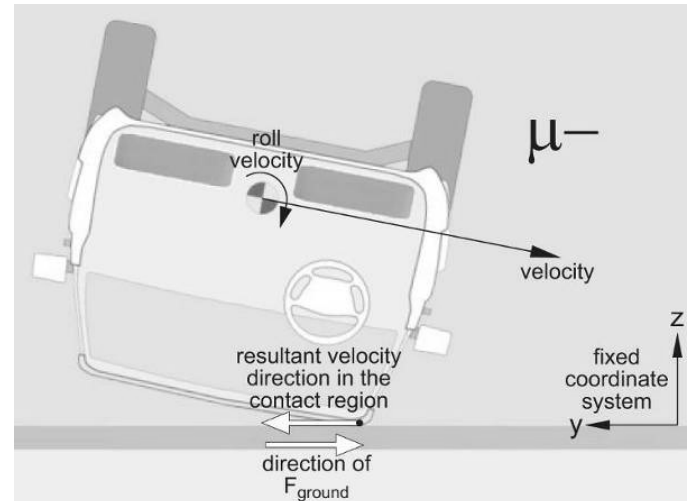


Figure 6b

For any particular vehicle-to-ground impact, there is a critical value of the impulse ratio,  $\mu_c$ , which will cause relative motion between the vehicle and the ground to cease in the contact region. The impulse ratio will not take on a value that exceeds this critical impulse ratio. Therefore, the magnitude of the available friction coefficient relative to the magnitude of the critical impulse ratio for a particular impact will have physical significance.

The available friction coefficient represents the magnitude of friction force that can be recruited during the impact. The critical impulse ratio represents the magnitude of friction force that must be recruited in order for relative motion to cease along the ground surface in the contact region between the vehicle and the ground. When the critical impulse ratio is greater than the available friction coefficient, then all of the available friction will be recruited during the impact, but that friction will be insufficient to cause sliding to cease in the contact region. When the available friction coefficient exceeds the critical impulse ratio, only a portion of the available friction will be recruited and sliding will cease in the contact region. In such cases, the value of the impulse ratio for the impact model should be set at the value of the critical impulse ratio, not the available friction coefficient. This is because recruitment of the available friction depends on relative velocity being present between the ground and the vehicle body. Once this relative motion ceases, no additional friction can be recruited. These concepts can be summarized as follows:

$$\text{If } \mu_c > \mu_{\text{available}}, \text{ then } \mu = \mu_{\text{available}}.$$

$$\text{If } \mu_c < \mu_{\text{available}}, \text{ then } \mu = \mu_c.$$

The critical impulse ratio for any particular vehicle-to-ground impact is the value of the impulse ratio that results in the final velocity at the Point C being zero, as follows:

$$v_{yc,f} = v_{y,f} + r \cdot s\phi \cdot \omega_{r,f} = 0 \quad (7)$$

To determine how the critical impulse ratio is influenced by the impact conditions and vehicle properties, the authors derived an analytical expression for the critical impulse ratio, which is given by Equation (8) below. The derivation of Equation (8) is detailed in Appendix A.

$$\mu_c = \frac{[(1+e) \cdot v_{zc,i} - g\Delta t] \cdot (r^2 \cdot s\phi \cdot c\phi) + v_{yc,i} \cdot (k_r^2 + r^2 \cdot c^2\phi)}{[(1+e) \cdot v_{zc,i} - g\Delta t] \cdot (k_r^2 + r^2 \cdot s^2\phi) + v_{yc,i} \cdot (r^2 \cdot s\phi \cdot c\phi)} \quad (8)$$

As this equation shows, the critical impulse ratio depends on the following factors: (1) the vehicle's initial velocity conditions for the impact; (2) the coefficient of restitution; (3) the impact duration; (4) and the impact configuration and geometry (which can include the deformed shape of the vehicle). The authors used Equation (8) to calculate critical impulse ratios for a number of impact scenarios. Some of these scenarios are shown graphically in Figure 7.

In this graph, the vehicle's OTG speed is plotted on the horizontal axis and the critical impulse ratio on the vertical axis. The impact scenarios depicted in this graph are for a vehicle CoM downward speed of 2 mph, a roll velocity of 300 degrees per second, a radius of gyration for the roll axis of 2.04 feet, an impact radius of 3.0 feet, a coefficient of restitution of 0, and an impact duration of 300 milliseconds. The motivation for selecting these values is discussed in Reference 28. The graph contains curves for impact angles of 60, 70, 80 and 90 degrees.

This graph demonstrates that for a fixed roll velocity and impact configuration, the critical impulse ratio will decrease as the vehicle's OTG speed decreases. For the sake of illustration, consider a situation in which the available friction coefficient can be assumed to be 0.5. If this is the case, then Figure 8 shows the value which the impulse ratio would take on for each of the impact scenarios of Figure 7.

For all of the impact scenarios occurring at OTG speeds above 25 mph, the critical impulse ratio exceeds the available friction coefficient. Thus, for these scenarios, the impulse ratio takes on a value of 0.5. As the OTG speed drops below 25 mph, impact scenarios begin to arise in which the critical impulse ratios are less than the available friction. In these cases, the impulse ratio takes on the value of the critical impulse ratio.

As it turns out, these concepts surrounding the critical impulse ratio are central to explaining certain aspects of the dynamics of high-speed rollover crashes. In the sections that follow, we will describe the typical shape of the roll velocity history for a vehicle during a high-speed rollover and will show, first, that the behavior of the critical impulse ratio provides a physical explanation for this shape, and second, that there is a direct link between the shape of the roll velocity history for the vehicle and the OTG deceleration history for the vehicle. In fact, we will contend that the roll velocity history for the vehicle provides the best means for a reconstructionist to setup realistic variations in the vehicle's deceleration rate over the course of the roll distance.

### The Influence of OTG Speed and Impact Angle on the Critical Impulse Ratio

( $v_{z,i} = 2$  mph,  $\omega_{r,i} = 300$  deg/s,  $k_r = 2.04$  ft,  $r = 3.0$  ft,  $e = 0$ ,  $\Delta t = 300$  ms)

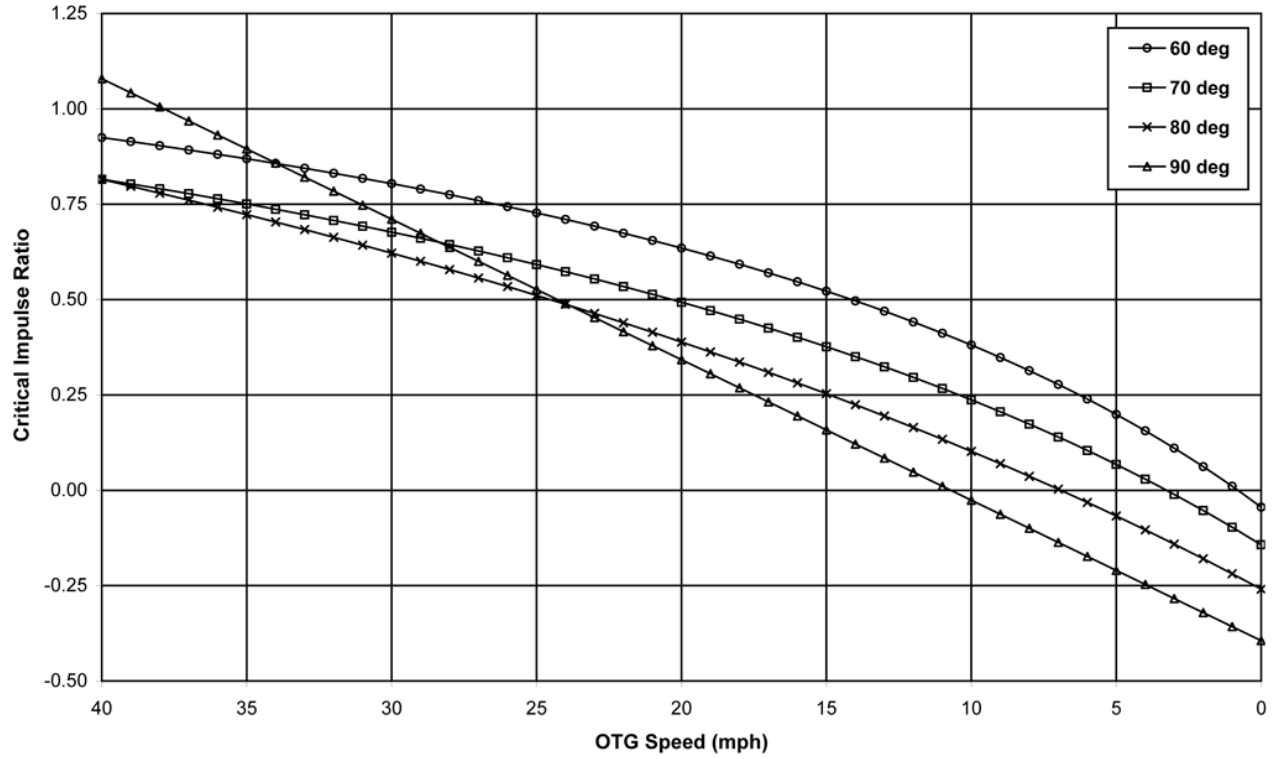


Figure 7

### The Influence of OTG Speed and Impact Angle on the Impulse Ratio

( $v_{z,i} = 2$  mph,  $\omega_{r,i} = 300$  deg/s,  $k_r = 2.04$  ft,  $r = 3.0$  ft,  $e = 0$ ,  $\Delta t = 300$  ms,  $\mu_{available} = 0.5$ )

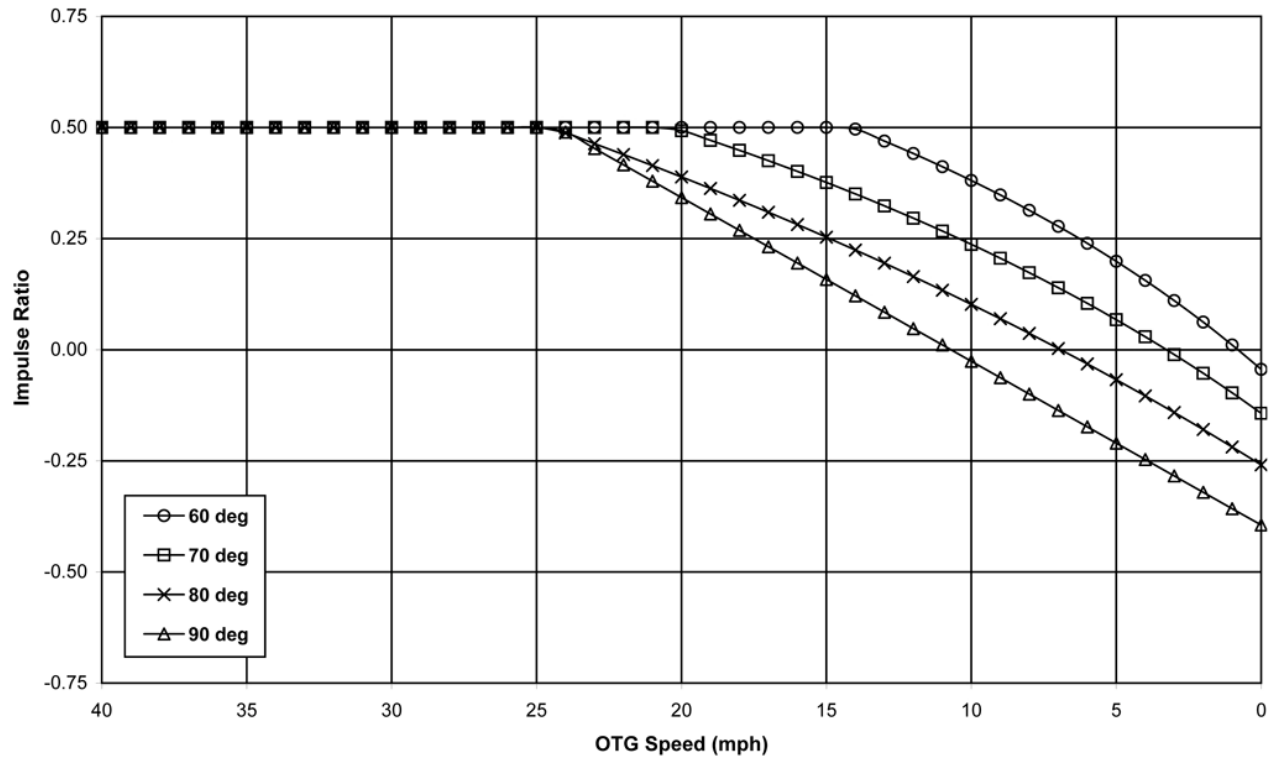


Figure 8

## ROLL VELOCITY HISTORY CHARACTERISTICS

Reference 26 discussed the dynamics of 12 real-world rollover crashes that were captured on video. The characteristics of these crashes provide a basis on which to explore the shape of typical roll velocity histories for high-speed rollover crashes. For instance, consider the dynamics of Case #3 from Reference 26, a high-speed, multiple-roll, crash involving a GMC Yukon Denali. Figure 9 contains frames from the video of this case showing the roll motion of the vehicle in this crash. Based on analysis of this video, the authors estimated that this vehicle rolled for approximately 144 feet and

that it had a translational speed at the beginning of the roll of 48 mph (average deceleration rate = 0.53).

Figure 10 depicts the roll velocity curve for this crash, plotted with the progression of the 3-¼ rolls that the vehicle experienced. After completing ¼-roll, the roll velocity of the vehicle was around 200 degrees per second. By the time the vehicle completed its first roll, the roll velocity had increased to around 450 degrees per second. Roll velocities exceeding 400 degrees per second were then maintained nearly through the third roll. From that point forward, the roll velocity generally decreased until the vehicle came to rest.



Figure 9

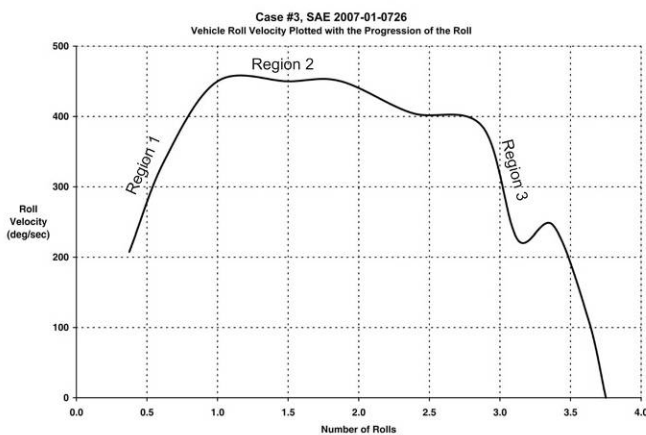


Figure 10

The roll velocity history for this crash is similar to that for other high-speed, multiple roll crashes that the authors presented in Reference 26. For instance, consider the roll velocity histories for Case Numbers 1, 6, 7 and 11, shown in Figure 11. In each of these cases, the roll velocity reached a moderate level after the vehicle completed about ¼-roll (the beginning of the roll phase), then built up to a high roll velocity level (400 deg/sec or

higher). For three out these four cases, high roll velocities are then maintained for some period of time before the roll velocity begins to diminish prior to the vehicle coming to rest.

These roll velocity histories can conceptually be split into the following three regions:

- **Region 1** – In this region, the vehicle’s roll velocity builds up from its level coming out of the trip phase to a peak or near-peak level.
- **Region 2** – In this region, the roll velocity reaches a plateau, with high roll velocities generally maintained and the vehicle experiencing only small increases or decreases in roll velocity.
- **Region 3** – In this region, the roll velocity steadily diminishes until the vehicle comes to rest.

These regions have been identified on the roll velocity histories of Figure 10 and 11.

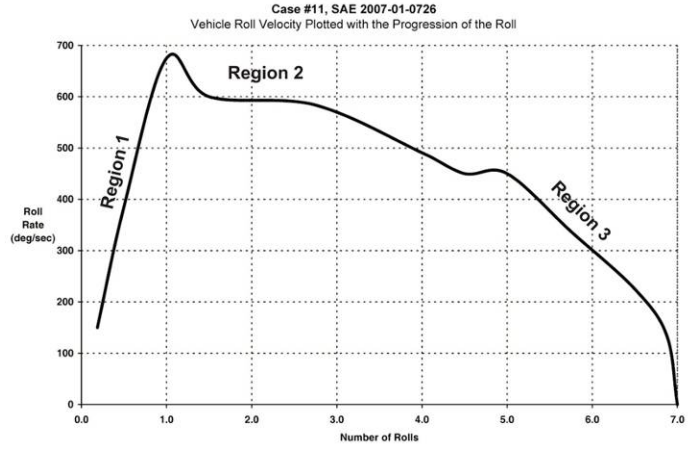
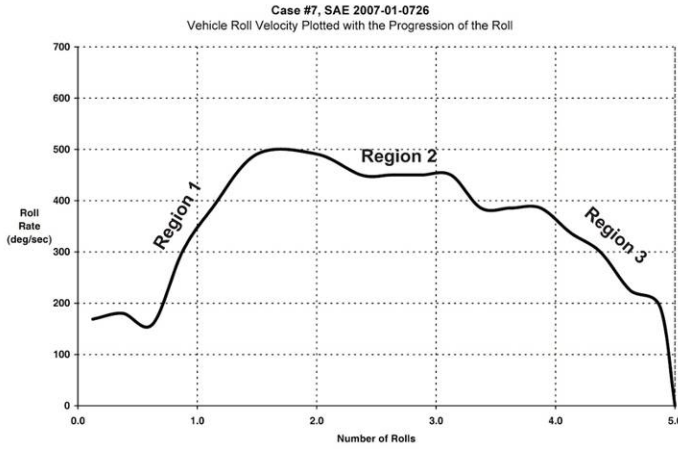
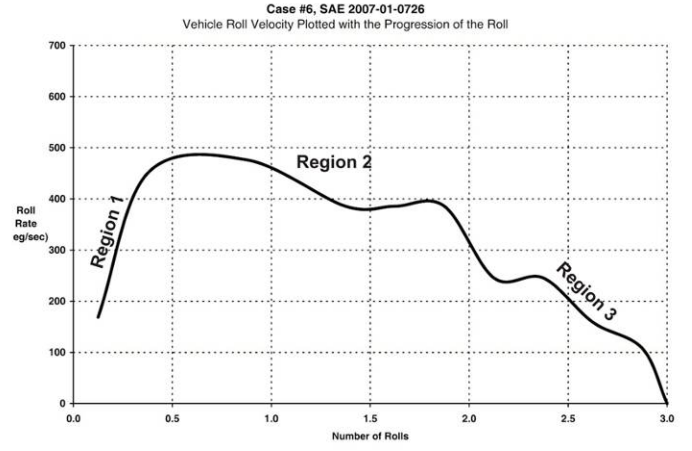
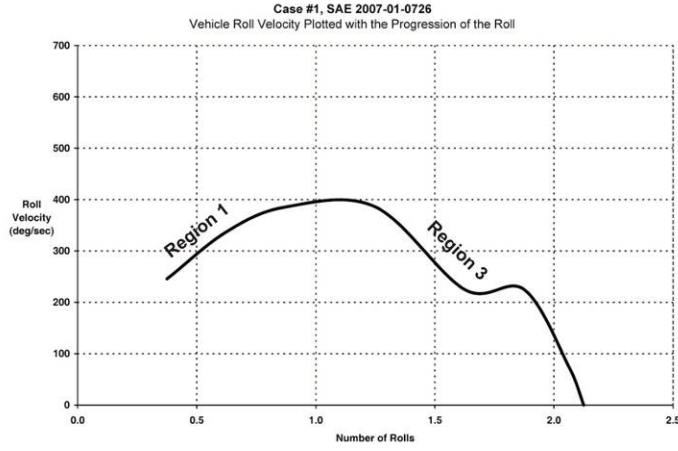


Figure 11

In Reference 28, the authors offered an explanation of the physics underlying a three-region roll velocity history. Because this three-region shape will play a role in our later discussion of how and why a rolling vehicle's deceleration rate varies over the course of a rollover, that explanation will be reviewed here.

Begin by reexamining Equation (3), which yields the change in roll velocity for a vehicle-to-ground impact:

$$\Delta\omega_r = (\Delta V_z + g \cdot \Delta t_i) \cdot \frac{r \cdot (\mu \cdot s\phi - c\phi)}{k_r^2} \quad (3)$$

In this equation, the sign of the  $\mu \cdot s\phi - c\phi$  term will vary with the impulse ratio and the impact angle and will determine whether the vehicle's roll velocity will increase or decrease. To see the physical meaning of this term, consider again the idealized vehicle-to-ground impact depicted in Figure 5. As this figure shows, during a vehicle-to-ground impact, there are three forces applied to the vehicle – the vehicle's weight and the ground surface and vertical components of the impact force. It is the moments applied to the vehicle by the components of the impact force that determine whether the roll velocity will increase or decrease as a result of the impact.

When the sum of the moments applied to the vehicle by the ground surface and vertical components of the impact force are positive, the roll velocity will increase and, when it is negative, the roll velocity will decrease. Thus, the roll velocity will increase when

$$F_{ground} \cdot r \cdot s\phi - F_{vertical} \cdot r \cdot c\phi > 0 \quad (9)$$

Multiplying Equation (9) by the impact duration  $\Delta t$  yields Equation (10):

$$P_{ground} \cdot r \cdot s\phi - P_{vertical} \cdot r \cdot c\phi > 0 \quad (10)$$

In Equation (10),  $P_{ground}$  and  $P_{vertical}$  are the ground plane and vertical impulses applied to the vehicle during the impact. By definition,

$$\mu = \frac{P_{ground}}{P_{vertical}} \quad (11)$$

Equation (11) can be substituted into Equation (10) and it can then be simplified to yield the following condition under which a vehicle-to-ground impact will yield an increase in roll velocity:

$$\mu \cdot s\phi - c\phi > 0 \quad (12)$$

The condition of Equation (12) is equivalent to the sign controlling term of Equation (3). Thus, this condition relates physically to the balance of moments applied to the vehicle by the impact force components.

Now, consider Figure 12, which shows the manner in which this  $\mu \cdot s\phi - c\phi$  term varies with the vehicle's OTG speed for impact angles varying between 60 and 90 degrees. In this graph, the vehicle's OTG speed is plotted on the horizontal axis and the value of the  $\mu \cdot s\phi - c\phi$  term is plotted on the vertical axis. The impact scenarios depicted in this graph are for a vehicle CoM downward speed of 2 mph, a roll velocity of 300 degrees per second, a radius of gyration for the roll axis of 2.04 feet, an impact radius of 3.0 feet, a coefficient of restitution of

0.00, and an impact duration of 300 milliseconds. The impact scenarios in Figure 12 assume an available friction coefficient of 0.75.

For each of the curves of Figure 12, the  $\mu \cdot s\phi - c\phi$  term begins at the high speed end of the horizontal axis with its maximum values. As the OTG speed drops, moving toward the right on the horizontal axis, the  $\mu \cdot s\phi - c\phi$  term maintains its maximum value for a range of speeds that depends on the impact angle, and then its value begins to drop. At the higher speeds, all of the impact angles result in a positive value for this term. As the speeds drop, these positive values are maintained, but their magnitudes drop. As the OTG speeds continue to drop, the values taken on by the  $\mu \cdot s\phi - c\phi$  term become negative, and increasingly so as the speed approaches zero.

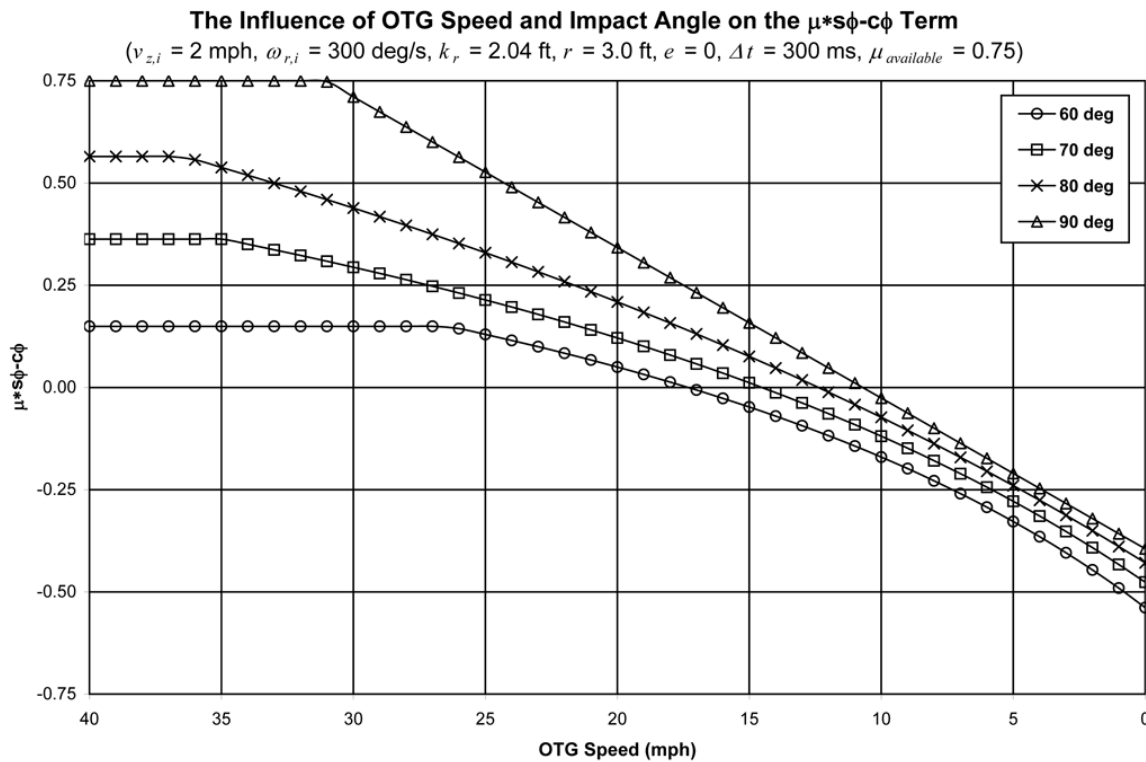


**Figure 12**

This pattern is what underlies the three-region shape of the typical roll velocity history for a high-speed rollover. At high translational speeds, most possible impact scenarios result in the vehicle experiencing an increase in roll velocity. In the moderate speed range, the vehicle may experience increases or decreases in roll velocity, but the magnitude of these will tend to be lower than in the high-speed region. In the low speed region, the vehicle will begin to experience only decreases in roll velocity, with the magnitude of these decreases become larger as the speed reaches zero. This trend will push the rollover towards termination as the vehicle's OTG speed reaches zero.

This trend in the roll velocity changes experienced by the vehicle can be observed in Figure 13, which is a graph plotting the changes in roll velocity for each of the impact scenarios of Figure 12. The vehicle's OTG speed is plotted on the horizontal axis and its change in roll velocity is plotted on the vertical axis. At higher OTG speeds, all of the impact scenarios result in significant increases in roll velocity. At moderate OTG speeds, impact scenarios result in relatively small increases or decreases in roll velocity. At low OTG speeds, impact scenarios result in significant decreases in roll velocity.

For the scenarios of Figure 13, the speed regions during which the three regions of the typical roll velocity curve would be produced can be identified. We have done

this in Figure 14. For these specific scenarios, the high speed region includes any speeds above, say, 20 mph. The moderate speed region includes speeds between 20 and 10 mph. The low speed region includes speeds below 10 mph. There is, of course, nothing sacred about these particular speeds. For any particular rollover, the speeds that constitute the boundaries of the three

regions will vary with the surface properties and the specific impact conditions that are realized. In the context of reconstruction, the delineation of the three regions of the roll velocity history should be driven by the specific physical evidence on that case and the speeds associated with the boundaries of the three regions will vary from case to case.

**The Influence of OTG Speed and Impact Angle on the Change in Roll Velocity**

( $v_{z,i} = 2$  mph,  $\omega_{r,i} = 300$  deg/s,  $k_r = 2.04$  ft,  $r = 3.0$  ft,  $e = 0$ ,  $\Delta t = 300$  ms,  $\mu_{available} = 0.75$ )

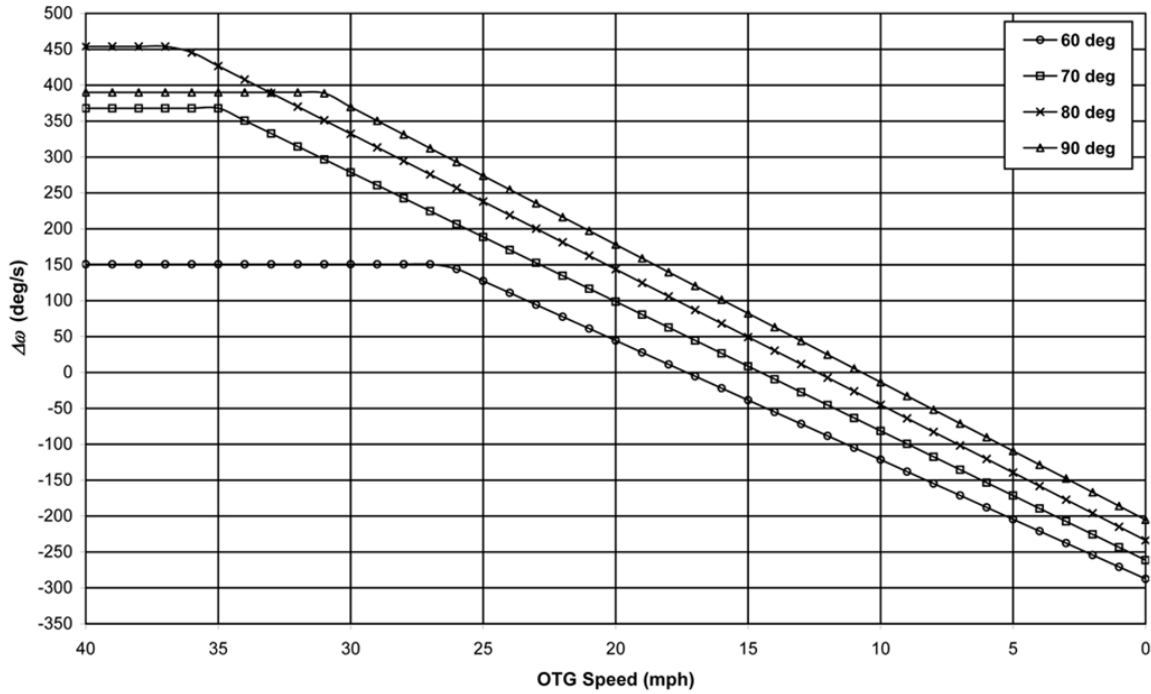


**Figure 13**

**The Influence of OTG Speed and Impact Angle on the Change in Roll Velocity**

( $v_{z,i} = 2$  mph,  $\omega_{r,i} = 300$  deg/s,  $k_r = 2.04$  ft,  $r = 3.0$  ft,  $e = 0$ ,  $\Delta t = 300$  ms,  $\mu_{available} = 0.75$ )

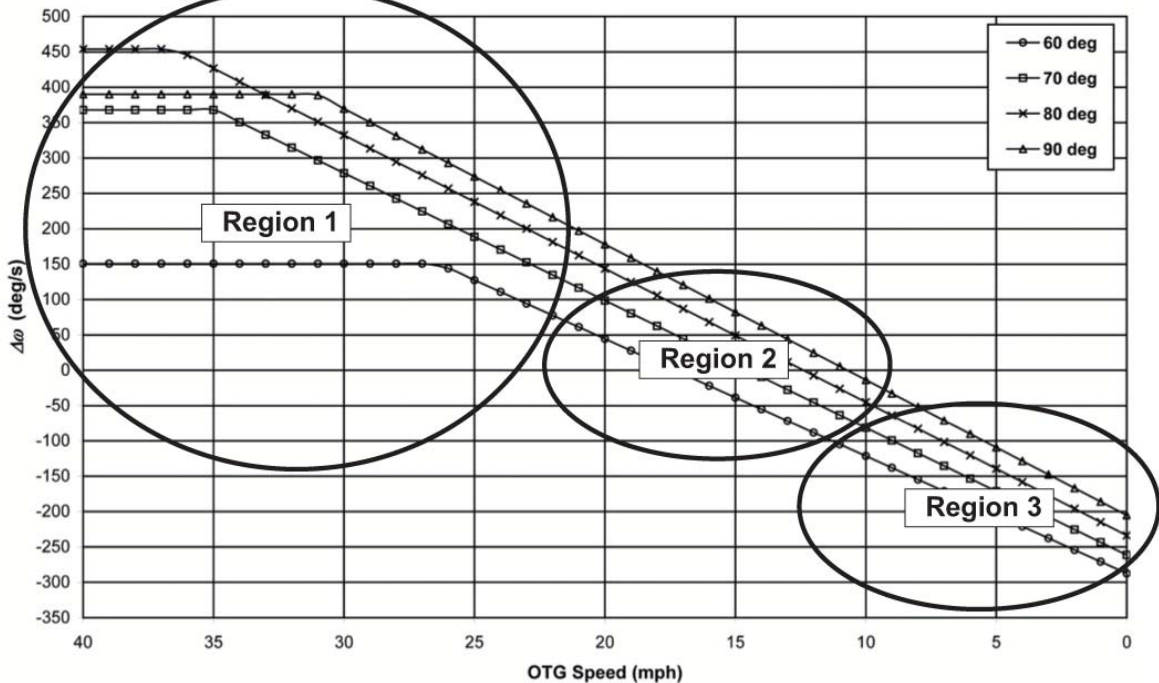


**Figure 14**

## DECELERATION DURING A GROUND IMPACT

The following equation will yield a vehicle's average OTG deceleration rate for a particular vehicle-to-ground impact:

$$f_{\text{impact}} = \left[ \frac{k_r^2}{r} \right] \cdot \left[ \frac{\mu}{\mu \cdot s\phi - c\phi} \right] \cdot \left[ \frac{\Delta\omega_r}{g\Delta t} \right] \quad (13)$$

In this equation,  $f_{\text{impact}}$  is the average ground plane deceleration rate for the vehicle during the vehicle-to-ground impact. To obtain Equation (13), Equation (3) was substituted into Equation (2) and the result was divided through by  $g\Delta t$ . This equation reveals the dependence of  $f_{\text{impact}}$  on the impulse ratio, the impact configuration, the roll inertia of the vehicle, the change in roll velocity and the impact duration. Equation (13) is significant for understanding how a vehicle's deceleration rate would vary over the course of a rollover because it reveals a relationship between the change in roll velocity experienced by the vehicle during a ground impact and the deceleration rate it experiences during that same impact. This indicates a relationship between the vehicle's roll velocity history and its over-the-ground deceleration rate history. This relationship can be exploited to develop a physically realistic method for a reconstructionist to vary a vehicle's deceleration rate over the course of a rollover.

To see this, consider Figures 15 through 17. Figure 15 is a graph showing a number of vehicle-to-ground impact scenarios with the change in roll velocity plotted on the horizontal axis and the vehicle's average deceleration rate for the impact plotted on the vertical axis. The horizontal axis progresses from large increases in roll velocity to large decreases in roll velocity. Interpreted in the context of a three-region roll velocity history, we can observe that Region 1 would encompass the left portion of the graph, Region 2 the middle portion, and Region 3 the right portion. The graph contains curves for four different impact angles with impact scenarios having the following conditions: (1) downward CoM velocity, 2 mph; (2) initial roll velocity, 300 deg/s; (3) radius of gyration for the roll axis, 2.04 ft; (4) impact radius, 3.0 ft; (5) coefficient of restitution, 0; (6) impact duration, 300 ms; and (7) available friction coefficient, 0.5. For all of the impact angles depicted, the average deceleration rates associated with the impact scenarios diminishes as one moves from left to right on the graph. Again interpreted in the context of the typical three region roll velocity history, this would imply that the deceleration rates associated with impacts would decrease as the vehicle progresses through a three-region roll velocity history. Thus, the deceleration rate would start at its highest level and steadily diminish through the roll phase.

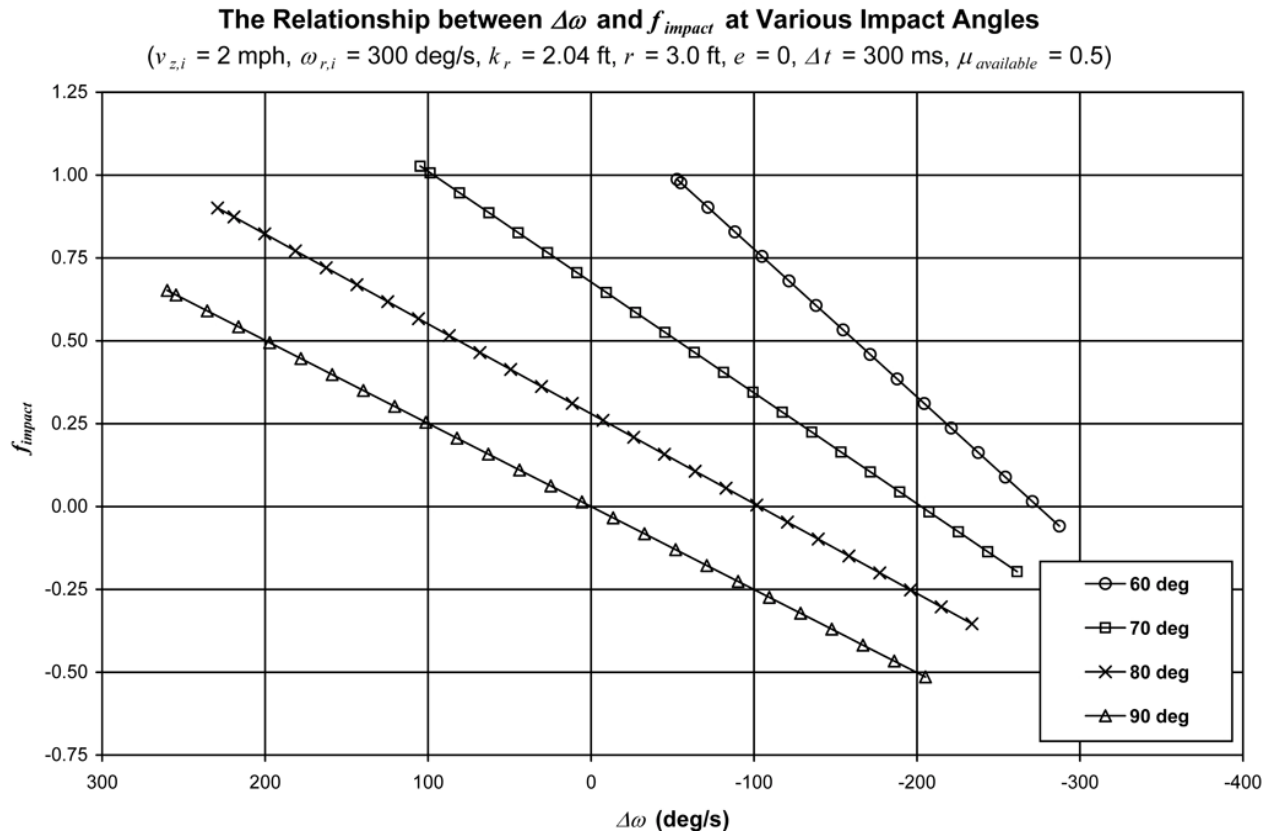


Figure 15

Figure 16 is another graph that depicts the same impact scenarios as those shown in Figure 15. Again, the change in roll velocity is plotted on the horizontal axis and the average deceleration rate for each impact is plotted on the vertical axis. However, in this instance, curves on the graph are associated with different OTG speeds, rather than different impact angles.

This graph reveals both the three-region behavior of the typical roll velocity history and the generally diminishing deceleration rates as the vehicle progresses through the rollover. Generally speaking, higher OTG speeds are associated with higher positive changes in roll velocity and with higher deceleration rates and lower speeds are associated with decreases in roll velocity and lower deceleration rates. It is significant to observe that the first curve in Figure 16 is associated with OTG speeds between 25 and 40 mph. Thus, for the impact scenarios shown, the deceleration rate does not begin to drop until the OTG speed drops below 25 mph.

Figure 17 is another graph that again depicts the same impact scenarios as those shown in Figure 15. In this case, the vehicle's OTG speed has been plotted on the horizontal axis and the average deceleration rate

associated with each impact has been plotted on the vertical axis. There are four separate curves on the graph, each associated with a different impact angle. On this graph, it is clear that the deceleration rates associated with the impacts are the highest in the high speed region. At some critical speed value, different for each impact angle, the deceleration rates begin to diminish.

Based on the trends shown in these graphs, we would propose that after the three (or perhaps two) regions of the roll velocity history have been delineated in terms of distance, that these same divisions can be used as points at which the vehicle's average deceleration rate would change (the discrete regions approach). Such regional variation could be prescribed in a number of ways. For instance, a different constant deceleration rate could be prescribed for each region (Figure 2). Alternatively, one could prescribe a linearly decreasing deceleration rate (Figure 3) or a deceleration rate profile similar to those depicted in Figure 17 where the deceleration rate would be high and constant in Region 1 and then linearly decrease through the second and third regions.

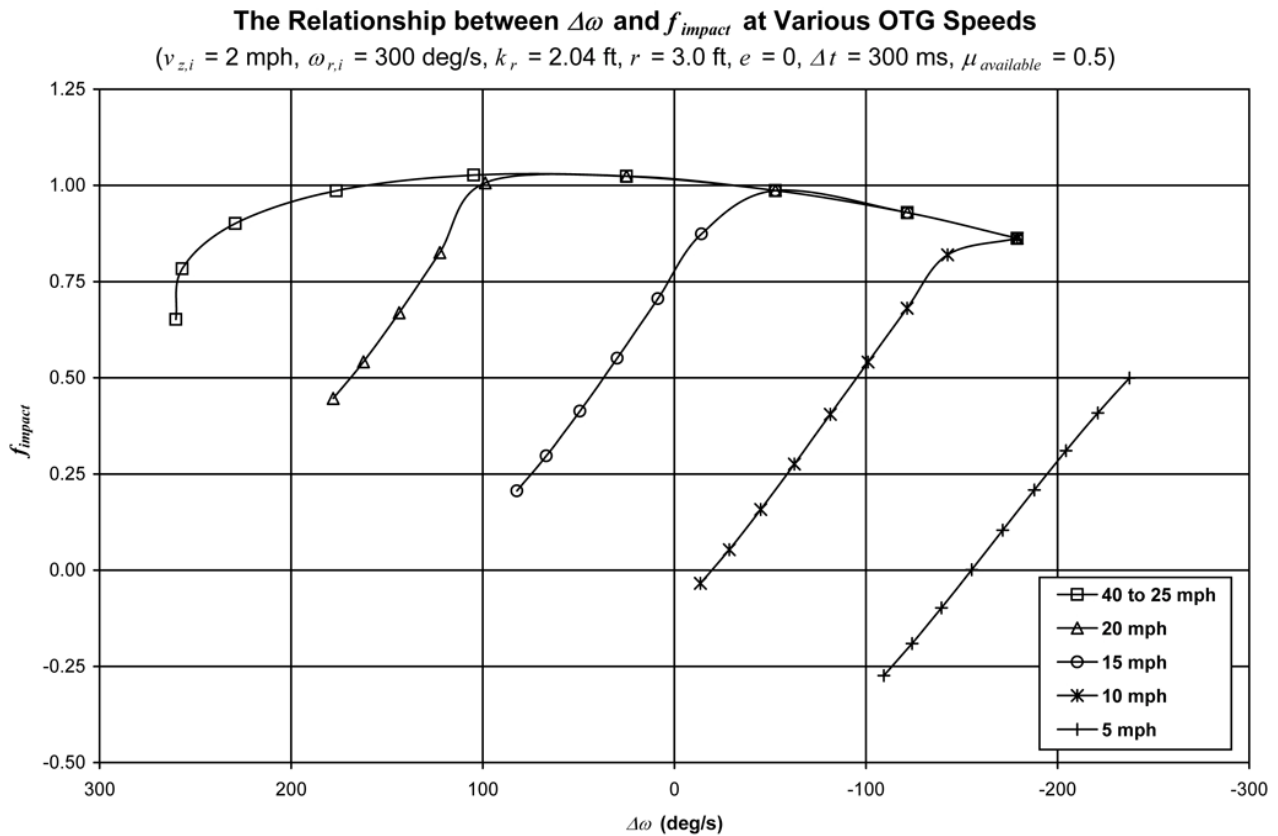


Figure 16

### The Influence of OTG Speed and Impact Angle on $f_{impact}$

( $v_{z,i} = 2$  mph,  $\omega_{r,i} = 300$  deg/s,  $k_r = 2.04$  ft,  $r = 3.0$  ft,  $e = 0$ ,  $\Delta t = 300$  ms,  $\mu_{available} = 0.5$ )

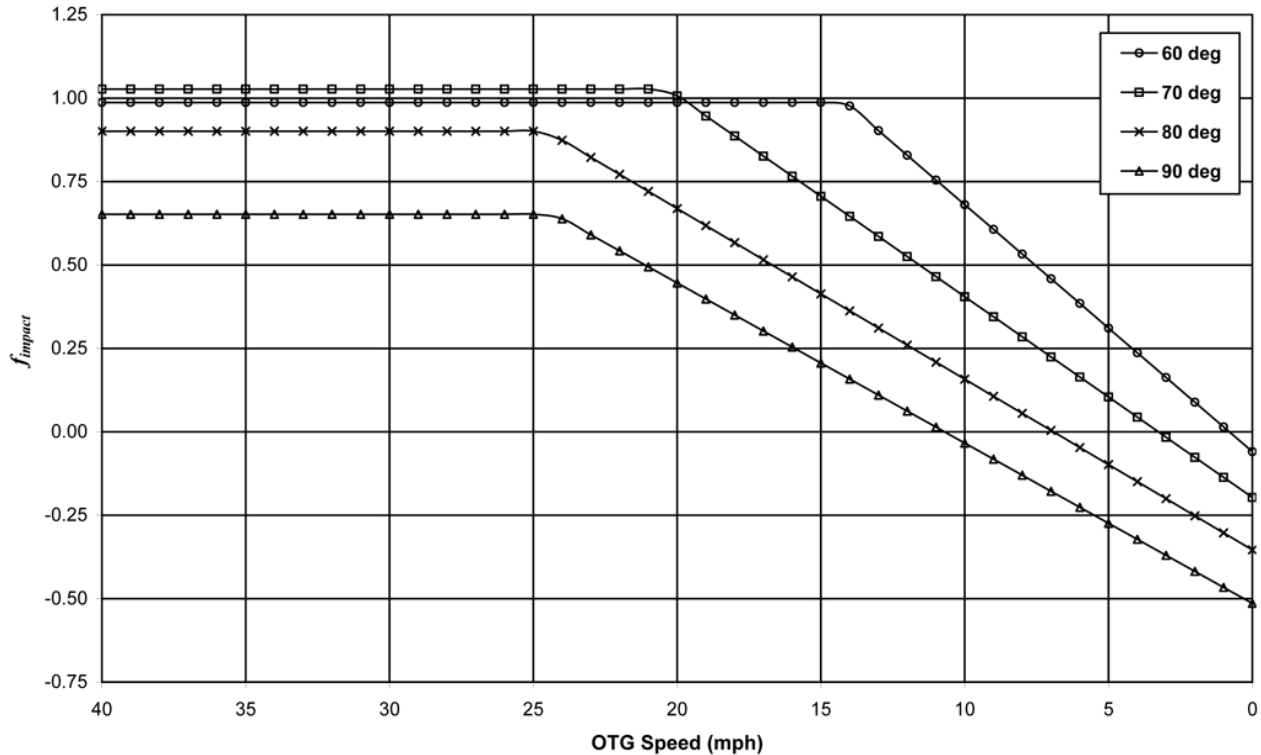


Figure 17

### COMPARISON WITH CRASH TEST DATA

To determine the degree to which using a variable deceleration rate approach would be expected to improve the accuracy of rollover reconstruction, the authors used various variable deceleration rate profiles to analyze two rollover crash tests. These crash tests were originally reported by Luepke in Reference 18, and then further analysis of these tests was reported by Luepke in Reference 19 and by Carter in Reference 9.

Both tests were dolly rollover tests conducted at the Exponent Test and Engineering Center in Phoenix, Arizona in a manner similar to that specified in SAE Recommended Practice J2114. This test procedure involves generating a lateral roll of the test vehicle by accelerating a dolly, on which the vehicle sits, up to the test speed, then decelerating that cart at a sufficient rate to initiate the rollover. The vehicle is situated on the cart perpendicular to the initial velocity direction with an initial roll angle of 23 degrees. In the tests under consideration here, the vehicles were situated on the dolly with their driver's sides leading. The vehicles were launched onto a 6" layer of lightly-compacted desert soil.

In the first test, which was run with a 1998 Ford Expedition, the test vehicle was launched at a speed of 43.2 mph. During this test, the vehicle rolled 4 times in approximately 120 feet, having an average deceleration rate over this distance of 0.52 g. The distance from the

time the vehicle first touched down coming off of the dolly to the time the vehicle came to rest was approximately 113 feet, and over this distance, the vehicle had an average deceleration rate of 0.55g.

In the second test, which was run with a 2004 Volvo XC90, the test vehicle was launched at a speed of 42.9 mph. During this test, the vehicle rolled 4-¼ times in approximately 115 feet, having an average deceleration rate over this distance of approximately 0.53 g. The distance from the time the vehicle first touched down coming off of the dolly to the time the vehicle came to rest was approximately 111.5 feet, and over this distance, the vehicle had an average deceleration rate of 0.55g.

Carter conducted a frame-by-frame analysis of the video footage of these tests and correlated the vehicle positions and orientations to the physical evidence deposited on the test surface [9]. Based on the spatial and temporal positions of the vehicles in these tests, Carter calculated OTG speed versus time curves for each of the tests. Carter obtained roll velocity curves for these tests from sensor data. In conducting our comparisons in this paper, we relied on this analysis previously conducted by Carter, utilizing his vehicle positions and orientations and his OTG speed and roll velocity versus time plots. In Reference 9, Carter showed the degree to which a constant deceleration rate approach would yield errors in the reconstruction. We

explored the degree to which various variable deceleration rate profiles could be used to reduce those errors.

For each test, we specified the following deceleration rate profiles, each having an overall average deceleration rate of 0.55g: (1) Constant: a constant deceleration rate of 0.55g; (2) Variable-Constant: a step function deceleration rate profile in which the deceleration rate leading up to peak roll velocity was set at a constant value greater than 0.55g and the deceleration rate following the peak roll velocity was set at a value less than 0.55g...the specific values of the deceleration rate before and after the peak roll velocity were chosen to visually minimize the error in the resulting OTG and roll velocities; (3) Linear: a linearly decreasing deceleration rate profile in which the deceleration rate began high and steadily progressed to a low value...again, the specific slope of this line was chosen to minimize the errors in the reconstruction; (4) Constant-Linear: a function that began with a high and constant deceleration rate, and then at the time of the peak roll velocity, began to decrease linearly...the initial deceleration rate and the later decrement of this rate were chosen to visually minimize the error in the resulting reconstruction.

Figures 18 and 19 are graphs showing the OTG speed versus time plots for each of these deceleration profiles for the Expedition test. The first graph (Figure 18) has a line titled "Test Data" showing the actual OTG speed versus time curve. This graph then includes the velocity curves for the "Constant" and "Variable Constant" deceleration rate profiles. In constructing the "Variable-Constant" curve in this case, the deceleration rate prior to the peak roll velocity was set at 0.84g and the deceleration rate after the peak roll velocity was set at 0.44g. The "Variable Constant" deceleration rate profile improves on the "Constant" deceleration rate in the early stages of the roll and in terms of the total time of the roll. Nonetheless, this profile still results in considerable underestimation of the velocities in the later stages of the rollover and of the total event duration.

The second graph (Figure 19) again has a line titled "Test Data" showing the actual OTG speed versus time curve. This graph then includes the velocity curves for the "Linear" and "Constant-Linear" deceleration rate profiles. In constructing the "Linear" deceleration rate profile for this case, the initial deceleration rate was set at 0.78g and the final deceleration rate was set at 0.29g. In constructing the "Constant-Linear" deceleration rate profile for this case, the initial deceleration rate was set at 0.73g and then from the time the vehicle passed the peak roll rate to the time it came to rest, the deceleration rate decreased linearly down to a value of 0.25g.

Both of these profiles represent a considerable improvement over the constant deceleration rate. The OTG speed errors are significantly reduced, though

there is still obvious underestimation of the OTG speeds in the later portions of the roll. The estimates of the overall event duration are excellent.

Figure 20 shows similar results for the roll velocity versus time plots for each of the variable deceleration profiles for the Expedition test. The constant deceleration rate yields the least accurate roll velocity curve. The "Variable-Constant" provides some improvement over the constant deceleration rate, but the "Linear" and "Constant-Linear" provide the most accurate roll velocity curves. All three variable deceleration rate profiles yielded good agreement with the peak roll velocity.

Similarly, Figures 21 and 22 are graphs showing the OTG speed versus time plots for each of these variable deceleration profiles for the XC90 test. The first graph (Figure 21) has a line titled "Test Data" showing the actual OTG speed versus time curve. This graph then includes the velocity curves for the "Constant" and "Variable Constant" deceleration rate profiles. The roll velocity curve in this case (see Figure 23 below) exhibited three regions. The first region encompassed the first  $\frac{3}{4}$  seconds of the roll during which the roll velocity built up to its peak value. The second region encompassed the time from  $\frac{3}{4}$  to about  $2\frac{1}{4}$  seconds, during which the roll velocity decreased. The third region encompassed the time after  $2\frac{1}{4}$  seconds during which the roll velocity decreased at a greater rate than it did during Region 2. Thus, in constructing the "Variable-Constant" curve in this case, a separate deceleration rate was specified for each of these regions. The deceleration rate for Region 1 was set at 0.76g; the deceleration rate for Region 2 was set at 0.39g; finally, the deceleration rate for Region 3 was set at 0.25g. In this case, the "Variable-Constant" deceleration rate profile represents a significant improvement over the "Constant" deceleration rate, particularly in the early stages of the roll. In fact, as the next figure will demonstrate, the "Variable-Constant" profile resulted in the best match with the OTG speed history in this case.

The next graph (Figure 22) again has a line titled "Test Data" showing the actual OTG speed versus time curve. This graph then includes the velocity curves for the "Linear" and "Constant-Linear" deceleration rate profiles. In constructing the "Linear" deceleration rate profile for this case, the initial deceleration rate was set at 0.80g and the final deceleration rate was set at 0.30g. In constructing the "Constant-Linear" deceleration rate profile for this case, the initial deceleration rate was set at 0.68g and then from the time the vehicle passed the peak roll rate to the time it came to rest, the deceleration rate decreased linearly down to a value of 0.29g.

Again, both of these profiles represent a considerable improvement over the constant deceleration rate. The OTG speed errors are significantly reduced, though there is still obvious overestimation of the OTG speed

early in the roll and underestimation of the OTG speeds in the later portions of the roll. The estimates of the overall event duration are again excellent.

Figure 23 shows results for the roll velocity versus time plots for each of the variable deceleration profiles for the XC90 test. Again, the constant deceleration rate yields the least accurate roll velocity curve. The “Linear” and “Constant-Linear” represent a significant improvement over the constant deceleration rate, but in this case, the “Variable-Constant” profile provides the most accurate roll velocity curve. All three variable deceleration rate profiles yielded acceptable agreement with the peak roll velocity.

The next graph (Figure 22) again has a line titled “Test Data” showing the actual OTG speed versus time curve. This graph then includes the velocity curves for the “Linear” and “Constant-Linear” deceleration rate profiles. In constructing the “Linear” deceleration rate profile for this case, the initial deceleration rate was set at 0.80g and the final deceleration rate was set at 0.30g. In constructing the “Constant-Linear” deceleration rate

profile for this case, the initial deceleration rate was set at 0.68g and then from the time the vehicle passed the peak roll rate to the time it came to rest, the deceleration rate decreased linearly down to a value of 0.29g.

Again, both of these profiles represent a considerable improvement over the constant deceleration rate. The OTG speed errors are significantly reduced, though there is still obvious overestimation of the OTG speed early in the roll and underestimation of the OTG speeds in the later portions of the roll. The estimates of the overall event duration are again excellent.

Figure 23 shows results for the roll velocity versus time plots for each of the variable deceleration profiles for the XC90 test. Again, the constant deceleration rate yields the least accurate roll velocity curve. The “Linear” and “Constant-Linear” represent a significant improvement over the constant deceleration rate, but in this case, the “Variable-Constant” profile provides the most accurate roll velocity curve. All three variable deceleration rate profiles yielded acceptable agreement with the peak roll velocity.

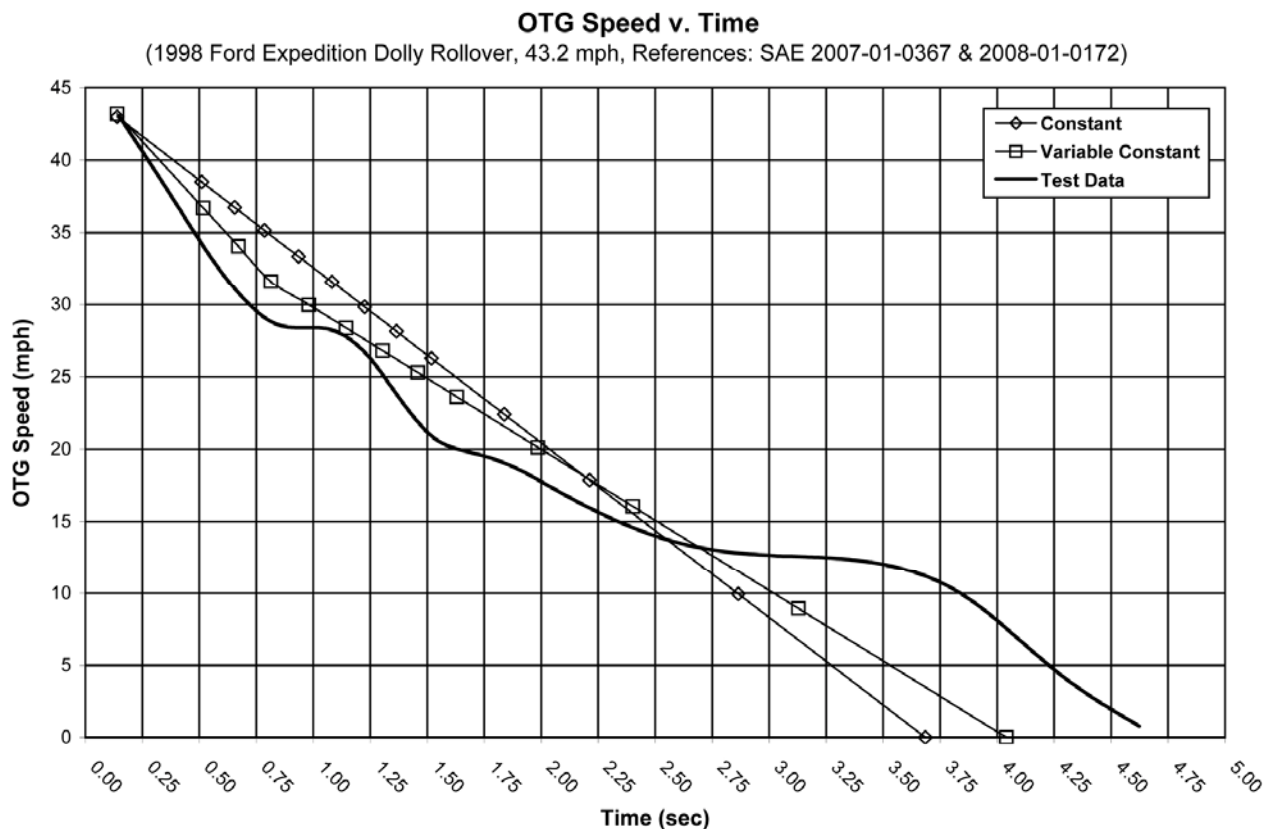


Figure 18

### OTG Speed v. Time

(1998 Ford Expedition Dolly Rollover, 43.2 mph, References: SAE 2007-01-0367 & 2008-01-0172)

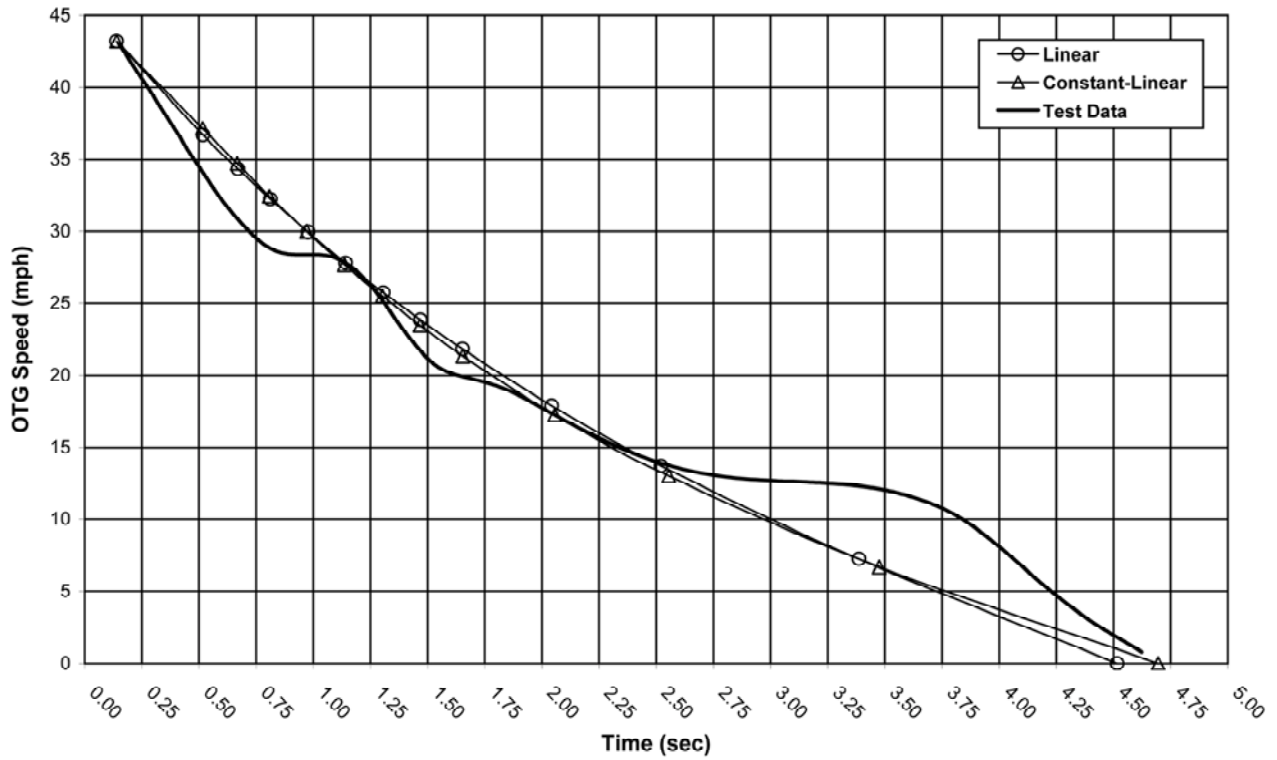


Figure 19

### Roll Velocity v. Time

(1998 Ford Expedition Dolly Rollover, 43.2 mph, References: SAE 2007-01-0367 & 2008-01-0172)

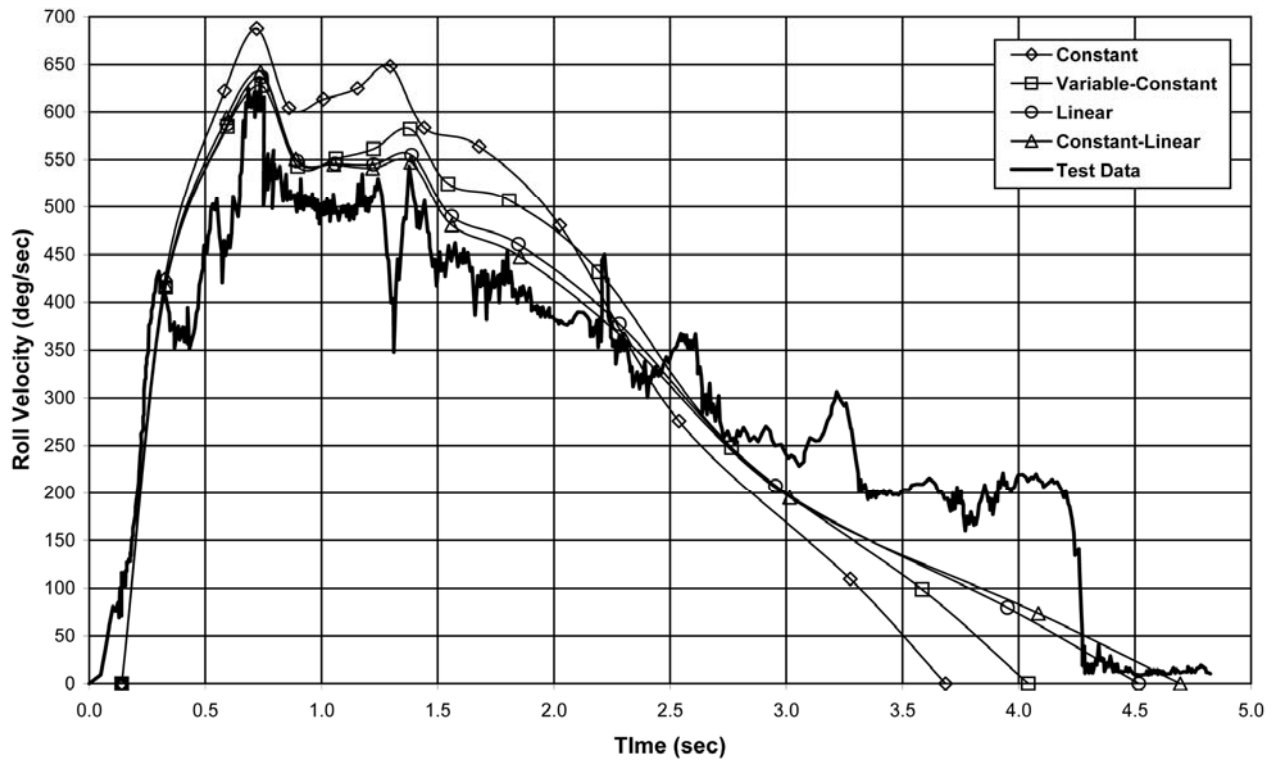
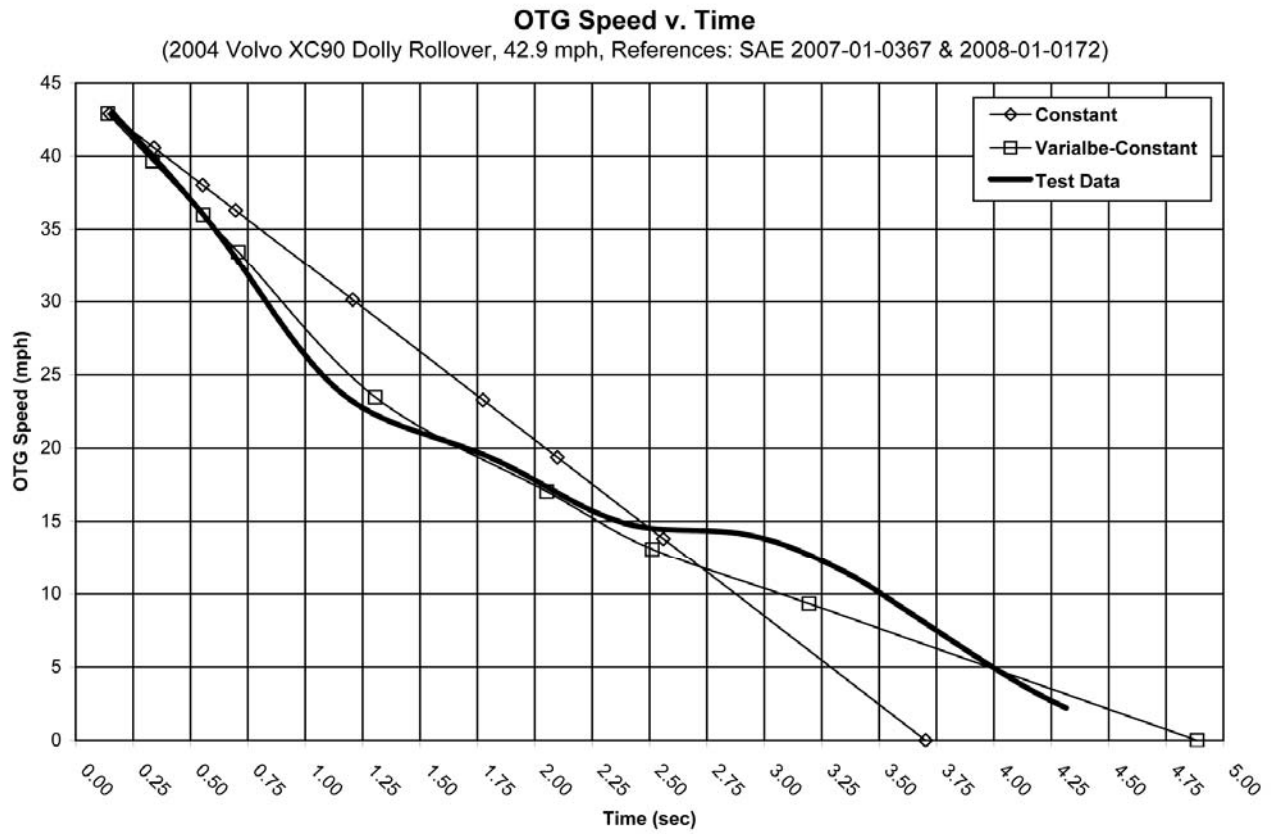
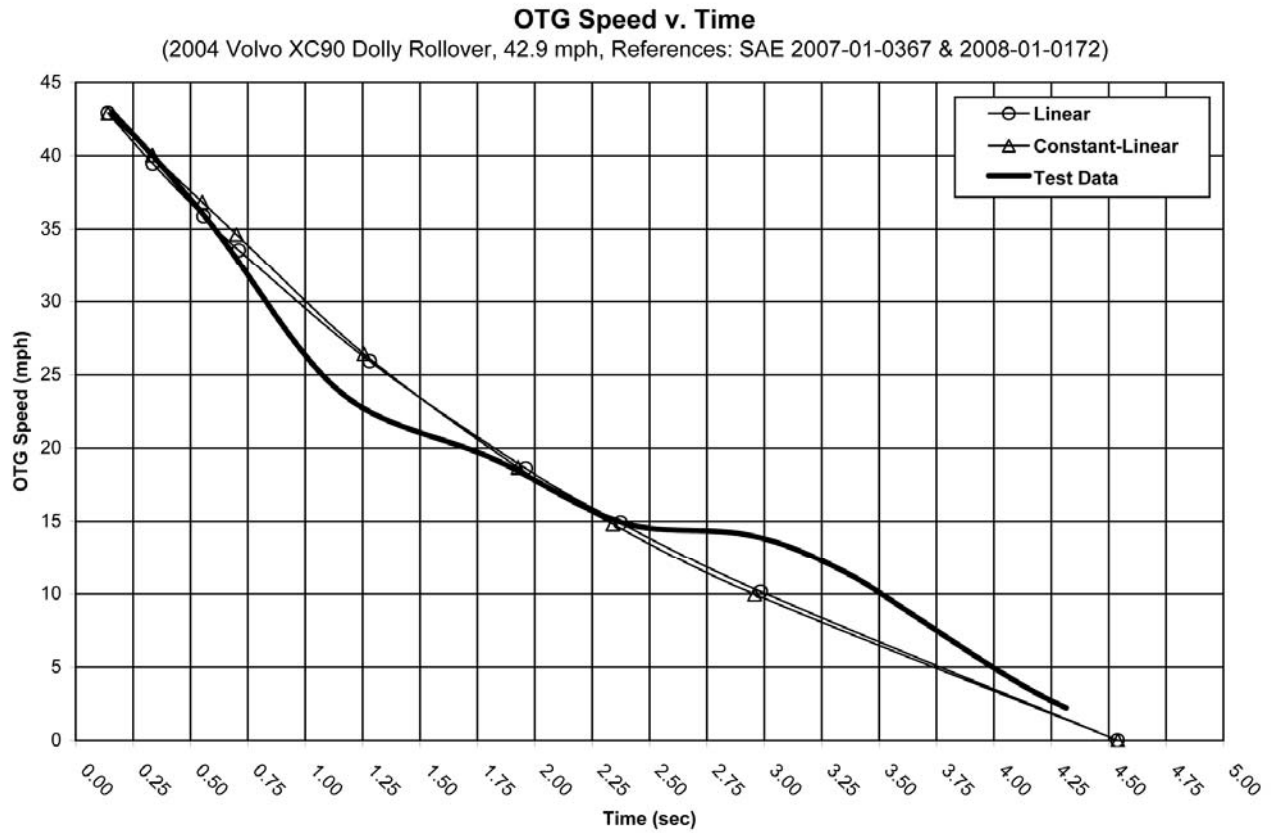


Figure 20



**Figure 21**



**Figure 22**

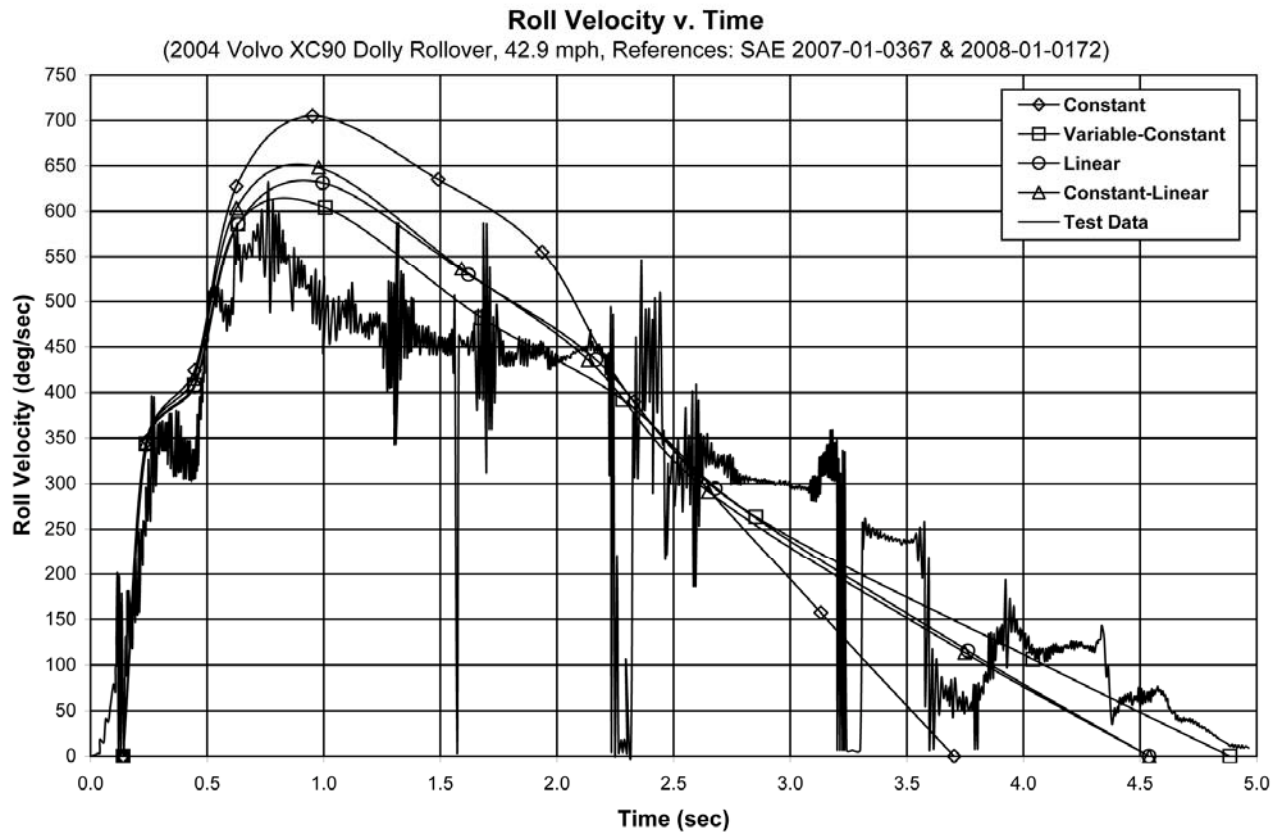


**Figure 23**

## DISCUSSION

The authors recommend the following procedure for reconstructing a rollover using a variable deceleration rate profile:

1. Spatially reconstruct the motion of the vehicle based on physical evidence deposited at the crash scene and on the crash vehicle [5, 21, 22].
2. Use a constant deceleration rate to generate an initial estimate of the OTG speed versus distance and roll velocity versus distance curves.
3. Identify the three (or two) regions of the roll velocity distance history in terms of the roll distance. Generate a variable deceleration rate profile that will yield the same average deceleration rate with which the initial estimate curves were generated.
4. Having generated a variable deceleration rate profile, recalculate the speed versus distance and roll velocity versus distance curves using the variable deceleration rate profile.

Clearly, this paper has not answered all of the questions that need to be answered to fully construct a variable deceleration rate approach to rollover reconstruction. For instance, suppose one specifies an average deceleration rate of 0.5 for a particular rollover and then

sets out to generate a variable deceleration rate profile that will yield that average deceleration rate. How high should the deceleration rate be in Region 1 and how low should it be in Region 3? Clearly there will be a range of reasonable values, but what are the boundaries of those ranges for each region. The crash tests examined in this paper provide some guidance on this front, but more work on this topic would certainly be productive.

In addition to such unanswered questions, it should also be stated that, while we have not explored a discrete events approach to generating a variable deceleration rate profile, it is possible that further research could make such an approach feasible. In fact, we anticipate that such an approach will be explored by other authors in the forthcoming literature related to rollover reconstruction. Clearly, a discrete events approach will require well documented physical evidence since the analyst will have to parse out specifically when the vehicle is in contact with the ground and when it is not.

## REFERENCES

1. Anderson, J.D., et al., "Analysis of a Real-World High-Speed Rollover Crash from a Video Record and Physical Evidence," SAE Technical Paper Number 2008-01-1486.

2. Ashby, Blake, et al., "Compressive Neck Preloading During the Airborne Phase of Vehicle Rollover," SAE Technical Paper Number 2007-01-0377.
3. Bahling, G.S., et al., "Rollover and Drop Tests – The Influence of Roof Strength on Injury Mechanics Using Belted Dummies," SAE Technical Paper Number 902314.
4. Brach, Raymond M., Mechanical Impact Dynamics: Rigid Body Collisions, 2007. This reference is available at [www.brachengineering.com](http://www.brachengineering.com).
5. Brach, Raymond M., Brach, R. Matthew, Vehicle Accident Analysis and Reconstruction Methods, SAE, 2005.
6. Brach, Raymond M., Brach, R. Matthew, "A Review of Impact Models for Vehicle Collision," SAE Technical Paper Number 870048.
7. Brach, Raymond M., Brach, R. Matthew, "Energy Loss in Vehicle Collision," SAE Technical Paper Number 871993.
8. Brach, Raymond M., "An Impact Moment Coefficient for Vehicle Collision Analysis," SAE Technical Paper Number 770014.
9. Carter, Jarrod W., Peter Luepke, Kevin C. Henry, Geoff J. Germane, James W. Smith, "Rollover Dynamics: An Exploration of the Fundamentals," SAE Technical Paper Number 2008-01-0172.
10. Chen, H. Fred, Guenther, Dennis A., "Modeling of Rollover Sequences," SAE Technical Paper Number 931976.
11. Christoffersen, Steven R., et al., "Deceleration Factors on Off-Road Surfaces Applicable for Accident Reconstruction," SAE Technical Paper Number 950139.
12. Funk, James R., et al., "Occupant Ejection Trajectories in Rollover Crashes: Full-Scale Testing and Real World Cases," SAE Technical Paper Number 2008-01-0166.
13. Funk, James R., et al., "Trajectory Model of Occupants Ejected in Rollover Crashes," SAE Technical Paper Number 2007-01-0742.
14. Gloeckner, D. Claire, et al., "Timing of Head-to-Vehicle Perimeter Contacts in Rollovers," SAE Technical Paper Number 2007-01-0370.
15. Henry, Kevin C., "Soft Surface Roll Mechanics for Light Vehicle Rollover Accident Reconstruction," Master's Thesis, Brigham Young University, August 2007.
16. Hughes, Raymond J., et al., "A Dynamic Test Procedure for Evaluation of Tripped Rollover Crashes," SAE Technical Paper Number 2002-01-0693.
17. Keifer, Orion P., "Vehicle Linear and Rotational Acceleration, Velocity and Displacement during Staged Rollover Collisions," SAE Technical Paper Number 2007-01-0732.
18. Luepke, Peter, et al., "An Evaluation of Laminated Side Window Glass Performance During Rollover," SAE Technical Paper Number 2007-01-0367.
19. Luepke, Peter A., et al., "Rollover Crash Tests on Dirt: An Examination of Rollover Dynamics," SAE Technical Paper Number 2008-01-0156.
20. Marine, Micky C., "On the Concept of Inter-Vehicle Friction and Its Application in Automobile Accident Reconstruction," SAE Technical Paper Number 2007-01-0744.
21. Martinez, J. Ed, Schlueter, Richard J., "A Primer on the Reconstruction and Presentation of Rollover Accidents," SAE Technical Paper Number 960647.
22. Meyer, Steven E., et al., "Accident Reconstruction of Rollovers – A Methodology," SAE Technical Paper Number 2000-01-0853.
23. Newberry, William N., et al., "A Computational Analysis of the Airborne Phase of Vehicle Rollover: Occupant Head Excursion and Head-Neck Posture," SAE Technical Paper Number 2005-01-0943.
24. Orlowski, K. Bundorf, R.T., Moffatt, E.A., "Rollover Crash Tests – The Influence of Roof Strength on Injury Mechanics," SAE Technical Paper Number 851734.
25. Orlowski, K.F., Moffatt, E.A., Bundorf, R.T., Holcomb, M.P., "Reconstruction of Rollover Collisions," SAE Technical Paper Number 890857.
26. Rose, Nathan A., Beauchamp, Gray, Fenton, Stephen J., "Factors Influencing Roof-to-Ground Impact Severity: Video Analysis and Analytical Modeling," SAE Technical Paper Number 2007-01-0726.
27. Rose, Nathan A., Beauchamp, Gray, Fenton, Stephen J., "Analysis of Vehicle-to-Ground Impacts During a Rollover with an Impulse-Momentum Impact Model," SAE Technical Paper Number 2008-01-0178.
28. Rose, Nathan A., et al., "The Influence of Vehicle-to-Ground Impact Conditions on Rollover Dynamics

and Severity,” SAE Technical Paper Number 2008-01-0194.

Rollovers,” SAE Technical Paper Number 2007-01-0366.

29. Warner, Charles Y., et al., “Friction Applications in Accident Reconstruction,” SAE Technical Paper Number 830612.
30. Warner, Mark H., Charles Y. Warner, Charles L. Crosby, “Roadway Asphalt Damage Force Analysis for Accident Reconstruction,” SAE Technical Paper Number 2008-01-0173.
31. Yamaguchi, Gary T., “Theoretical Analysis of a Method of Computing Dynamic Roof Crush During

## CONTACT

Nathan Rose  
Kineticcorp, LLC  
6070 Greenwood Plaza Blvd., Suite 200  
Greenwood Village, Colorado 80111  
(303) 733-1888  
nrose@kineticcorp.com  
www.kineticcorp.com

## APPENDIX A – DERIVATION OF CRITICAL IMPULSE RATIO EQUATION

Equations (2) and (3) can be combined to obtain the following equation:

$$\Delta\omega_r = \frac{r \cdot (\mu \cdot s\phi - c\phi)}{\mu \cdot k_r^2} \cdot \Delta V_y \quad (A1)$$

Equations (6) and (10) can be combined to obtain the following equation:

$$\Delta V_{y,c} = \Delta V_y + r \cdot s\phi \cdot \Delta\omega_r \quad (A2)$$

Substituting Equation (A1) into (A2) yields the following equation:

$$\Delta V_{y,c} = \Delta V_y \left[ \frac{\mu \cdot k_r^2 + r^2 \cdot s\phi \cdot (\mu \cdot s\phi - c\phi)}{\mu \cdot k_r^2} \right] \quad (A3)$$

Substituting Equation (2) into Equation (A3) yields the following equation:

$$\Delta V_{y,c} = [\Delta V_z + g \cdot \Delta t] \cdot \left[ \frac{\mu \cdot k_r^2 + r^2 \cdot s\phi \cdot (\mu \cdot s\phi - c\phi)}{k_r^2} \right] \quad (A4)$$

Substituting Equation (1) into Equation (A4) yields the following equation:

$$\Delta V_{y,c} = - \left[ \begin{array}{l} (1+e) \cdot v_{zc,i} \cdot \left\{ \frac{k_r^2}{k_r^2 - r^2 \cdot c\phi \cdot (\mu \cdot s\phi - c\phi)} \right\} \\ - g \cdot \Delta t \cdot \left\{ 1 + \frac{r^2 \cdot c\phi \cdot (\mu \cdot s\phi - c\phi)}{k_r^2 - r^2 \cdot c\phi \cdot (\mu \cdot s\phi - c\phi)} \right\} \end{array} \right] \cdot \left[ \frac{\mu \cdot k_r^2 + r^2 \cdot s\phi \cdot (\mu \cdot s\phi - c\phi)}{k_r^2} \right] \quad (A5)$$

Simplifying algebraically results in the following equation:

$$\Delta V_{y,c} = -[(1+e) \cdot v_{zc,i} - g \cdot \Delta t] \cdot \left[ \frac{\mu \cdot k_r^2 + r^2 \cdot s\phi \cdot (\mu \cdot s\phi - c\phi)}{k_r^2 - r^2 \cdot c\phi \cdot (\mu \cdot s\phi - c\phi)} \right] \quad (A6)$$

Solving Equation (A6) for  $\mu$  results in the following equation:

$$\mu = \frac{\left( (1+e) \cdot v_{zc,i} - g\Delta t \right) \cdot (r^2 \cdot s\phi \cdot c\phi) - \Delta V_{y,c} \cdot (k_r^2 + r^2 \cdot c^2\phi)}{\left( (1+e) \cdot v_{zc,i} - g\Delta t \right) \cdot (k_r^2 + r^2 \cdot s^2\phi) - \Delta V_{y,c} \cdot (r^2 \cdot s\phi \cdot c\phi)} \quad (A7)$$

At the critical value of  $\mu$ ,  $\Delta V_{y,c} = -V_{y,ci}$ . Thus:

$$\mu_c = \frac{\left( (1+e) \cdot v_{zc,i} - g\Delta t \right) \cdot (r^2 \cdot s\phi \cdot c\phi) + v_{y,ci} \cdot (k_r^2 + r^2 \cdot c^2\phi)}{\left( (1+e) \cdot v_{zc,i} - g\Delta t \right) \cdot (k_r^2 + r^2 \cdot s^2\phi) + v_{y,ci} \cdot (r^2 \cdot s\phi \cdot c\phi)} \quad (A8)$$

Substituting Equations (4) and (6) yields the following equation:

$$\mu_c = \frac{\left( (1+e) \cdot (v_{z,i} - r \cdot c\phi \cdot \omega_{r,i}) - g\Delta t \right) \cdot (r^2 \cdot s\phi \cdot c\phi) + (v_{y,i} + r \cdot s\phi \cdot \omega_{r,i}) \cdot (k_r^2 + r^2 \cdot c^2\phi)}{\left( (1+e) \cdot (v_{z,i} - r \cdot c\phi \cdot \omega_{r,i}) - g\Delta t \right) \cdot (k_r^2 + r^2 \cdot s^2\phi) + (v_{y,i} + r \cdot s\phi \cdot \omega_{r,i}) \cdot (r^2 \cdot s\phi \cdot c\phi)} \quad (A9)$$

## APPENDIX B – CALCULATING AN AVERAGE DECELERATION RATE

In Reference 9, Carter observes that, for the two tests he analyzed, “average accelerations computed from the OTG acceleration traces (0.44g for Test 1 and 0.45g for Test 2) were at least 0.1g lower than the constant deceleration values used to match the speed at first contact. The much lower average acceleration would suggest that the terminology commonly used in the reconstruction community may be somewhat misleading.

“Typically the term average acceleration is used to describe the acceleration value used in the constant acceleration model. In reality the deceleration used to compute the speed at trip should be termed the effective deceleration or drag factor as opposed to the average. The effective deceleration or drag factor, at least based on the analysis presented here, is not the same as the average acceleration.”

Whatever one decides about the best terminology for accident reconstruction, the underlying reason for the difference noted by Carter has to do with the difference between using time-based and distance-based averages. The average acceleration obtained from a time-based acceleration trace will be different than the average acceleration obtained by calculating the average acceleration necessary to yield the correct initial speed based on the roll distance. For the purposes of accident reconstruction, average deceleration rates calculated based on rollover crash test data should be calculated based on the overall roll distance, not the overall roll time. This is because the use of physical evidence, spatially located, dictates a distance based approach. Roll segment distances are known, or can be reconstructed, whereas the times associated with those distances must be calculated.

To see why this is the case, consider the difference between a distance-based average deceleration rate and a time-based average deceleration rate, in the context of a variable deceleration rate approach. Under

such an approach, a distance would be assigned to each of the three regions delineated by the roll velocity history and the average rollover deceleration rate would be calculated as follows:

$$f_{avg} = \frac{f_1 d_1 + f_2 d_2 + f_3 d_3}{d_{total}} \quad (B1)$$

In this equation,  $d_1$ ,  $d_2$  and  $d_3$  are the distances covered by the vehicle during each of the three regions and  $f_1$ ,  $f_2$  and  $f_3$  are the deceleration rates that the analyst assigns to each of these regions. To see the relationship between the average deceleration rate of Equation (B1) and a time-based average deceleration rate, consider the following series of equations.

Assuming a constant deceleration rate over the Region 3 roll distance, the velocity at the beginning of the Region 3 is given by Equation (B2).

$$v_3 = \sqrt{2f_3 g d_3} \quad (B2)$$

The time associated with Region 3 can then be estimated with Equation (B3).

$$t_3 = \frac{v_3}{f_3 g} \quad (B3)$$

Combining Equations (B2) and (B3) through  $v_3$  yields the following equation relating  $d_3$  and  $t_3$ :

$$d_3 = \frac{f_3 g t_3^2}{2} \quad (B4)$$

Assuming a constant deceleration rate over the Region 2 distance, the velocity at the beginning of Region 2 is given by Equation (B5).

$$v_2 = \sqrt{2f_2gd_2 + v_3^2} \quad (\text{B5})$$

The time associated with Region 2 can then be estimated with Equation (B6).

$$t_2 = \frac{v_2 - v_3}{f_2g} \quad (\text{B6})$$

Combining Equations (B5) and (B6) yields the following equation relating  $d_2$  to  $t_2$  and  $t_3$ :

$$d_2 = \frac{f_2gt_2^2}{2} + f_3gt_2t_3 \quad (\text{B7})$$

A similar equation can be developed for  $d_1$ , given by Equation (B8).

$$d_1 = \frac{f_1gt_1^2}{2} + f_2gt_1t_2 + f_3gt_1t_3 \quad (\text{B8})$$

Substituting Equations (B4), (B7) and (B8) into Equation (B1) yields the following equation that relates the average deceleration rate, calculated using the roll distance, to the region durations.

$$f_{avg} = \sqrt{\frac{f_1^2t_1^2 + 2f_1f_2t_1t_2 + 2f_1f_3t_1t_3 + f_2^2t_2^2 + 2f_2f_3t_2t_3 + f_3^2t_3^2}{t_{total}^2}} \quad (\text{B9})$$